

RESEARCH ARTICLE

# Kinematics and singularity analysis of a novel hybrid industrial manipulator

Sadanand Modak  and Rama Krishna K

Department of Mechanical Engineering, Indian Institute of Technology Delhi, New Delhi, India

**Corresponding author:** Sadanand Modak; Email: [modaksada11@gmail.com](mailto:modaksada11@gmail.com)

**Received:** 2 May 2022; **Revised:** 15 November 2023; **Accepted:** 16 November 2023;

**First published online:** 14 December 2023

**Keywords:** hybrid manipulator; 3-UPU; forward kinematics; inverse kinematics; singularity analysis; manipulability

## Abstract

This paper proposes a new type of hybrid manipulator that can be of extensive use in industries where translational motion is required while maintaining an arbitrary end-effector orientation. It consists of two serially connected parallel mechanisms, each having three degrees of freedom, of which the upper platform performs a pure translational motion with respect to the mid-platform. Closed-form forward and inverse kinematic analysis of the proposed manipulator has been carried out. It is followed by the determination of all of its singular configurations. The theoretical results have been verified numerically, and the 3D modeling and simulation of the manipulator have also been performed. A simple optimal design is presented based on optimizing the kinematic manipulability, which further demonstrates the potential of the proposed hybrid manipulator.

## 1. Introduction

Serial and parallel robot manipulators have had significant attention from academia. Serial manipulators are based on open kinematic chains, with the links being connected serially via different types of joints. They have been used in various industrial applications and elsewhere where there is a demand for large workspaces. On the other hand, parallel manipulators are based on closed-loop kinematic chains with a standard topological structure of two platforms (fixed base and moving) connected via multiple legs, where each leg is yet another serial chain. Owing to their parallel structure, they offer the advantages of higher stiffness, better operating speeds, and higher payload. However, they suffer from reduced as well as more complex overall workspace. A significant amount of research has been done on the design and kinematic analysis [1–5], as well as on the determination of workspace and singularities [1, 3, 5–13] of parallel manipulators. Based on different applications, numerous lower mobility parallel manipulators have been designed [1–5, 12, 13], in which the moving platform either purely translates [1–3, 12], or purely rotates [4, 5, 13], or else performs a combined translational and rotational motion [14]. A purely translational 3-DOF parallel manipulator named 3-UPU was first proposed by Tsai [2]. Di Gregorio et al. [1] further studied the geometric and assembly conditions necessary for the translational nature of a more general 3-RRPRR parallel manipulator in detail, with the 3-UPU being a special case of 3-RRPRR. The 3-UPU manipulator has three identical legs, each with two universal joints and a prismatic pair in U-P-U order. The 3-UPU wrist, having a pure spherical rotation of the platform with respect to the base, was proposed by Karouia et al. [4], which was further analyzed by Di Gregorio [5, 13].

A hybrid manipulator combines the advantages of serial and parallel manipulators in terms of having higher rigidity and a significantly larger workspace than a parallel manipulator, thereby offering a way to perform complex tasks. Due to this, there has been a growing interest in hybrid manipulators over the past few decades, even though the available literature is currently limited compared to serial and parallel manipulators. A hybrid manipulator is generally formed by combining serial and parallel structures. Quite a few serial–parallel-type hybrid manipulators have been proposed in the literature,

which are made up of parallel mechanisms connected in series. However, there are other type of hybrid manipulators as well consisting of multiple serial chains linked to a single parallel “base” (commonly seen in robotics). Shahinpoor [15] presented the kinematic analysis of a novel hybrid manipulator made by serially connecting two parallel manipulators. The inverse kinematics was completed by obtaining a set of nonlinear equations that must be solved numerically. Singh et al. [16] developed the complete kinematic model and determined the jacobian matrix of a 7-DOF spatial hybrid robotic arm for use in assisting a surgeon during medical surgery. Verification of the model was performed via a physical prototype. Maier and Woernle [17] presented a generalized inverse kinematic analysis of a cable-suspension hybrid manipulator comprising a 3-DOF cable-driven parallel mechanism and a 3-DOF serial mechanism. However, these hybrid manipulators require numerical solutions. A 6-DOF spatial manipulator with a novel architecture, designated as H6A (i.e., Hybrid 6-Axis), is discussed in ref. [18]. The manipulator consists of two arm-like branches attached to a rigid waist at one end and coupled through a wrist at the other end.

Romdhane [19] presented the kinematic analysis of a hybrid manipulator, again made up of two serially connected 3-DOF parallel mechanisms. The three successive prismatic joints in the lower mechanism restricted the motion of the mid-platform only to three translations. At the same time, the top platform performed spherical rotation about the mid-platform due to the existence of a spherical joint between the two platforms. Eight inverse kinematic solutions in closed form were obtained for the upper platform. Tanio Tanev [20] proposed a novel 6-DOF hybrid manipulator made up of two novel tripod mechanisms involving prismatic, revolute, and spherical joints. Closed-form forward and inverse kinematics were presented. Tanev obtained four forward kinematic solutions each for both the tripod mechanisms. Zheng et al. [21] utilized the two special 3-UPU mechanisms, which are the pure translational 3-UPU [2] and the pure rotational 3-UPU [4], and combined them serially such that the translational 3-UPU becomes the lower mechanism and the rotational 3-UPU becomes the upper mechanism. The forward position analysis of this new hybrid manipulator was carried out using quaternions, and two and eight solutions for the lower and upper mechanisms were obtained, respectively.

Gallardo-Alvarado et al. [22, 23] presented a novel topology for the 2(3-RPS) hybrid manipulator and approached its kinematic and dynamic analysis using screw theory. The simplicity and compactness of the expressions derived in the study were noted. Hu [24] presented a general approach to derive the unified forward and inverse Jacobian matrices for hybrid manipulators composed of lower mobility parallel manipulators connected serially. Huang et al. [25] proposed using a 3-DOF parallel mechanism as the main body of the 5-DOF “TriVariant” hybrid robot and discussed its design and synthesis. Its kinematic analysis was done, and observations about its performance were made. Lu et al. [26] proposed a novel hybrid manipulator composed of a 5-DOF parallel mechanism with two composite equivalent universal joints and three 1-DOF finger mechanisms. Its kinematics and dynamics are derived, and a 3D prototype of the proposed hybrid manipulator is also constructed and analyzed. Sangveraphunsiri and Chooprasird [27] proposed a 5-DOF hybrid manipulator having three translational and one rotational movement, with a single-axis rotating table. Its kinematics and dynamics are derived, where the latter is derived using the Lagrange formulation. Lingmin Xu et al. [28] presented a one-of-its-kind 3T1R 2-(PRR)-2-RH hybrid manipulator that uses two helical joints, having an equal but opposite pitch, connected to the moving platform, which imparts it full rotational capability. Peng Xu et al. [29] presented the kinematic analysis of a novel hybrid manipulator composed of mainly three parts: a 3-DOF translational parallel mechanism, a 2-DOF serial mechanism, and a turntable providing a redundant DOF. They noted its essential application in computer-controlled ultra-precision freeform polishing. A novel 5-DOF hybrid manipulator was proposed by Guo et al. [30], and its closed-form kinematic solutions were presented. More recently, He et al. [31] proposed a foldable 7-DOF hybrid manipulator to capture a noncooperative target in space. It has two parts, the upper part being a 4R serial mechanism and the lower part being a three-legged parallel manipulator with one UP leg and 2 UPS legs. In another work [32], a hybrid parallel–serial manipulator named CaHyMan (Cassino Hybrid Manipulator) is analyzed in terms of stiffness characteristics. From all these hybrid manipulators, it is clear that some hybrid

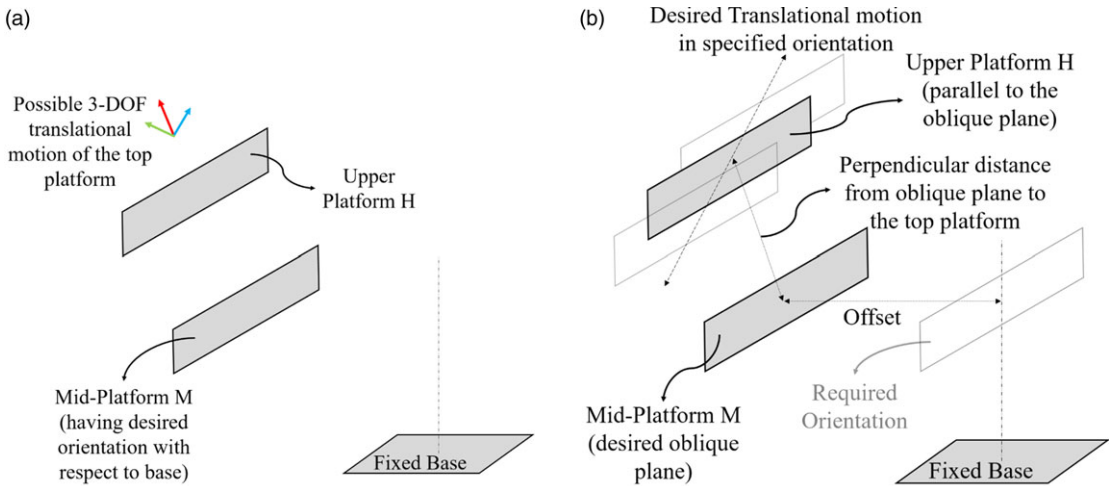


**Figure 1.** Conceptual representation of the motivation for the proposed hybrid manipulator. (a) 3-DOF pure translational capability of the upper platform H (it is a representative (i.e., conceptual) image since the platforms are, in reality, triangular and not rectangular). (b) Desired translational motion parallel to the oblique plane.

manipulators [19, 21] make it possible for the upper platform to have a pure 3-DOF rotational motion while maintaining some desired translation with respect to the base (due to the lower parallel mechanism being of pure translatory nature), but not the other way round.

However, in industries and manufacturing facilities, there is a frequent requirement of having a pure translational motion of the top platform with respect to an oblique plane at some arbitrary desired orientation with respect to the fixed base, such as in polishing, finishing, painting, or cleaning operations, especially where large structures are involved. One specific case could be of polyhedral domes or surfaces such as the geodesic dome or even the polyhedral structures used in deep space technology, including telescopes and satellites. Based on this motivation, this paper proposes a novel 6-DOF hybrid manipulator in which the top platform can perform 3-DOF pure translational motion with respect to any desired oblique plane (i.e., the mid-platform). This hybrid manipulator utilizes two 3-DOF parallel mechanisms: the lower one being the 1-RRR 2-SPS mechanism that resembles the tripod mechanism proposed by Tanev [20], and the upper one being the 3-UPU translational parallel manipulator (TPM) [2]. Although, the upper platform H of the proposed hybrid manipulator can perform a general 3-DOF pure translational motion with respect to the mid-platform while maintaining a constant orientation with respect to the fixed base as shown in Fig. 1(a), however, of particular interest and usefulness could be the special case of planar translation along a specified direction in a plane parallel to the desired oblique plane (i.e., mid-platform M) which is at some specified offset and orientation with respect to the fixed base. The schematic of this case is shown in Fig. 1(b). This desired motion can be decoupled and expressed in four parameters: the desired orientation + offset of the mid-platform with respect to the base, the perpendicular distance between the middle and the upper platform, and the desired translation direction. So, first, the lower parallel mechanism orients and translates simultaneously to achieve the desired pose (orientation and offset). After that, the upper parallel mechanism first attains the required perpendicular distance and then performs the desired translational motion in the specified direction in a plane parallel to the desired oblique plane. Note that the maximum possible offset value is constrained by the value of the revolute limb length of the lower parallel mechanism. The structure and configuration of the proposed hybrid manipulator allow for a convenient decoupling in its inverse kinematic analysis, which facilitates the attainment of closed-form solutions that, in turn, would make the control of this manipulator computationally efficient.

The remainder of this paper is organized as follows. The geometry and structure of the hybrid manipulator are described in Section 2. It is followed by its forward and inverse kinematic analysis in Sections 3 and 4, respectively. The 3D modeling, simulation, and numerical verification are presented in Section 5. Section 6 presents the singularities, while Section 7 lays the ground for more rigorous studies to get better optimal designs for the proposed hybrid manipulator.

## 2. Description of novel 6-DOF hybrid manipulator

### 2.1. Geometry and structure

The proposed hybrid manipulator, as shown in Fig. 2(a), consists of two 3-DOF parallel mechanisms connected serially, making it an overall 6-DOF hybrid manipulator. All the prismatic pairs ( $P_2, P_3, P_4, P_5, P_6$ ) and the  $R_2$  revolute joint are actuated (active). The two platforms, M and H, are taken to be equilateral, with circumradii of  $h_1$  and  $h_2$  ( $\neq h_1$ )<sup>1</sup>, respectively. The lower parallel mechanism resembles the upper parallel mechanism used by Tanev [20] in his hybrid manipulator. The lower parallel mechanism connects the base to the mid-platform M and comprises one RRR and two SPS legs. Here,  $axis(R_1)^2 \perp axis(R_2) \perp axis(R_3)$  and also  $axis(R_1) \perp \overline{B_1B_2}$  edge of the lower triangular base. Further,  $axis(R_3) \parallel \overline{M_1M_2}$  edge of the mid-platform. The upper parallel mechanism between the mid-platform M and the upper platform H (end-effector) is the standard 3-UPU TPM (also called the Tsai [2] manipulator) having three identical UPU legs. Tsai [2] first proposed the conditions required for the 3-UPU manipulator to perform pure translation, and later Gregorio et al. [1] derived the general TPM conditions using the proximal (modified) D-H convention [33], starting from the generic RRPRR<sup>3</sup> leg. This paper uses the distal (classical) D-H convention [34]. The distal form of the TPM conditions [1, 2] are imposed on the upper parallel mechanism in the following manner:

- $U_{1,1} \parallel U_{4,1}, U_{1,2} \parallel U_{4,2}, U_{2,1} \parallel U_{5,1}, U_{2,2} \parallel U_{5,2}$ , and  $U_{3,1} \parallel U_{6,1}, U_{3,2} \parallel U_{6,2}$ , where  $U_{ij}$  denotes the  $j$ th revolute joint axis (while traversing a limb upward, i.e., from bottom to the top) of the  $i$ th universal joint
- For each of the three UPU legs,  $\theta_3 = -\theta_2$  and  $\theta_4 = -\theta_1$ , where  $\theta_i$  is the rotation about the  $i$ th revolute joint of that particular limb while traversing upward
- $U_{1,2}, U_{2,2}$ , and  $U_{3,2}$  point toward the circumcenter of platform M
- $U_{4,1}, U_{5,1}$ , and  $U_{6,1}$  point toward the circumcenter of platform H
- $U_{1,2}$  and  $U_{4,1}$  are  $\perp axis(P_4)$ ,  $U_{2,2}$  and  $U_{5,1}$  are  $\perp axis(P_5)$  leg, and  $U_{3,2}$  and  $U_{6,1}$  are  $\perp axis(P_6)$  leg

The TPM conditions ensure that platform H does pure translation with respect to platform M. Thus, this structure of the hybrid manipulator allows the upper mechanism to perform pure translation motion while being in any desired orientation defined by the mid-platform M, with respect to the base. Furthermore, since the lower parallel mechanism can also translate, platform H can perform pure translation motion even in an oblique plane having some offset with respect to the base.

It is important to note that the choice of the lower mechanism as a 1-RRR 2-SPS mechanism provides the benefit of a straightforward and convenient interpretation for the Euler angles of the mid-platform M in terms of  $R_1, R_2$ , and  $R_3$  revolute joint angles. From the point of view of controlling the manipulator, this can be pretty useful as encoder feedback from the three revolute joints would directly give the orientation. Furthermore, choosing the upper mechanism as a translational 3-UPU mechanism decouples the orientation and translation of the top platform H, as now the orientation part is entirely governed by the lower mechanism actuators. This helps it achieve a fully closed-form solution structure. In addition to the various applications mentioned in Section 1, this proposed hybrid manipulator offers much flexibility

<sup>1</sup>Since  $h_1 = h_2$  gives a design singularity, as will be shown in Section 6.1.

<sup>2</sup>Where  $axis(R_i)$  is read as the axis of the joint  $R_i$ .

<sup>3</sup>Since a universal joint is equivalent to two perpendicular and intersecting revolute joints, UPU becomes a special case of RRPRR.

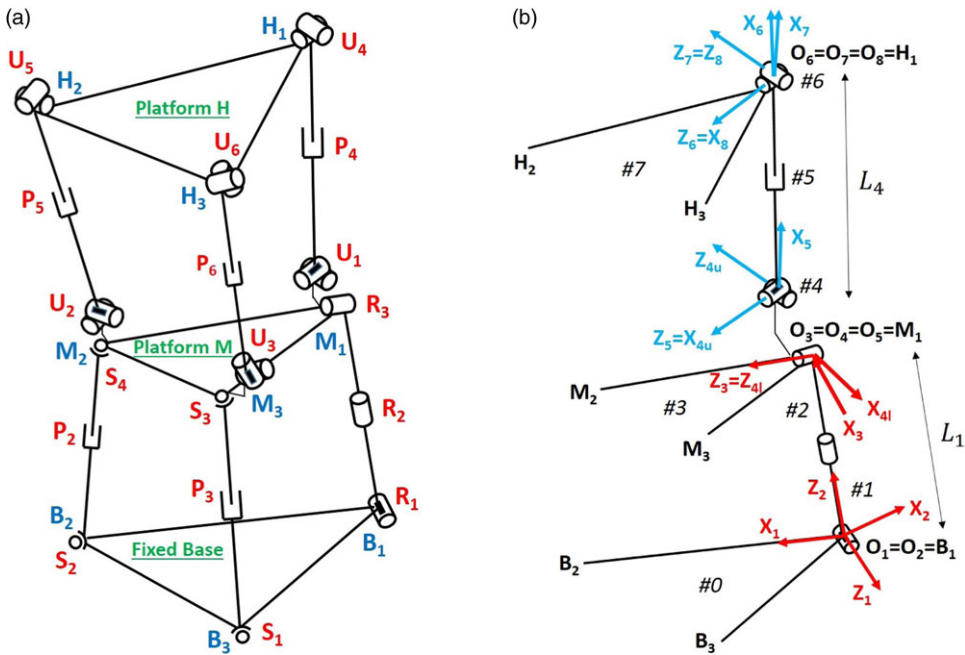


**Figure 2.** Proposed hybrid manipulator: (a) schematic (the centers of upper joints of the lower mechanism (i.e.,  $R_3$ ,  $S_4$ , and  $S_3$ ) coincide, respectively, with the centers of the lower joints of the upper mechanism (i.e.,  $U_1$ ,  $U_2$ , and  $U_3$ ). However, they have been depicted as separate for clarity), and (b)  $B_1M_1H_1$  limb with D-H frames.

as it can be converted to a standard 3-UPU manipulator just by fixing the lower mechanism, further diversifying its use cases. Finally, as seen in Section 7, even a basic optimization leads to a pretty good design obtaining relatively high manipulability for large parts of the motion range.

### 2.2. D-H analysis

The  $B_1M_1H_1$  limb of the hybrid manipulator with all the attached D-H coordinate frames is shown in Fig. 2(b). The frame 1 ( $X_1Y_1Z_1$ ) is attached to the fixed base (link #0), while the frame 8 is attached to the top moving platform H (link #7). Two separate frames  $4_l$  and  $4_u$  fixed to the middle platform M (link #3) are used for convenience in the analysis, which will be discussed in subsequent sections. Since the axes of the two revolute joints in a universal joint intersect, the lengths of links #4 and #6 are taken to be zero as they are the imaginary links connecting the two intersecting revolute joints of a universal joint. Let  $L_1 = B_1M_1$ ,  $L_2 = B_2M_2$ ,  $L_3 = B_3M_3$ ,  $L_4 = M_1H_1$ ,  $L_5 = M_2H_2$ , and  $L_6 = M_3H_3$ .<sup>4</sup>

Now, Table I represents the D-H table for the  $B_1M_1$  leg of the lower mechanism, and it transforms frame  $4_l$  to frame 1. Table II represents the D-H table for the  $M_1H_1$  leg of the upper mechanism after imposing the TPM conditions as listed in Section 2.1, and it transforms frame 8 to frame  $4_u$ . The intermediate (constant) rigid transformation matrix, which transforms frame  $4_u$  to  $4_l$  is

<sup>4</sup>Since  $L_1$  is a fixed limb length, it has to be positive always, but the prismatic limb lengths  $L_2, L_3, L_4, L_5$ , and  $L_6$  are signed variables and can take both positive and negative values, in theory. However, once the mechanism is assembled in a configuration with the prismatic limb lengths being positive, the negative limb lengths cannot be obtained physically without reassembling the manipulator. Henceforth, only the positive limb lengths have been considered in this paper.

**Table I.** D-H table for lower mechanism (along B<sub>1</sub>M<sub>1</sub> limb) of the proposed hybrid manipulator.

Link #i	b <sub>i</sub> (cm)	θ <sub>i</sub> (rad)	a <sub>i</sub> (cm)	α <sub>i</sub> (rad)
1	0	θ <sub>1</sub>	0	−π/2
2	L <sub>1</sub>	θ <sub>2</sub>	0	−π/2
3	0	θ <sub>3</sub>	0	0

**Table II.** D-H table for upper mechanism (along M<sub>1</sub>H<sub>1</sub> limb) of the proposed hybrid manipulator.

Link #i	b <sub>i</sub> (cm)	θ <sub>i</sub> (rad)	a <sub>i</sub> (cm)	α <sub>i</sub> (rad)
4	0	θ <sub>4</sub>	0	π/2
5	0	θ <sub>5</sub>	L <sub>4</sub>	0
6	0	−θ <sub>5</sub>	0	−π/2
7	0	−θ <sub>4</sub>	0	0

$$C_u^l = \begin{bmatrix} \frac{1}{2} & 0 & -\frac{\sqrt{3}}{2} & 0 \\ 0 & 1 & 0 & 0 \\ \frac{\sqrt{3}}{2} & 0 & \frac{1}{2} & 0 \\ 0 & 0 & 0 & 1 \end{bmatrix} \tag{1}$$

Now,  $T_1 = f(\theta_1, \theta_2, \theta_3)$  corresponds to the D-H Table I, while  $T_2 = f(\theta_4, \theta_5, L_4)$  corresponds to the D-H Table II. Therefore, the overall transformation matrix is written using the D-H Tables I and II as (details in Section A.1):

$$T = T_1 C_u^l T_2 = \begin{bmatrix} t_{11} & t_{12} & t_{13} & t_{14} \\ t_{21} & t_{22} & t_{23} & t_{24} \\ t_{31} & t_{32} & t_{33} & t_{34} \\ 0 & 0 & 0 & 1 \end{bmatrix} \tag{2}$$

Now, any position vector of a point expressed<sup>5</sup> in frame 8 can be transformed to the base frame using  $T$  from Eq. (2) as:

$${}^1p = T {}^8p = T_1 C_u^l T_2 {}^8p \tag{3}$$

It is to be noticed that the orientation part<sup>6</sup> of  $T$  depends *only* on  $\theta_1, \theta_2,$  and  $\theta_3,$  owing to the pure translational nature of the upper mechanism, which in turn facilitates the decoupling as shown later in Section 4.

### 3. Closed-form forward position analysis

In the direct kinematics problem, the values of all the active joints (here  $\theta_2, L_2, L_3, L_4, L_5, L_6$ ) are specified, and the pose (position + orientation) of the end-effector (upper platform H) needs to be determined. The pose of the end-effector can be entirely described by the overall transformation matrix  $T$  because

<sup>5</sup>In this paper, the left superscript denotes the frame of reference.

<sup>6</sup>The “orientation part” refers to the matrix made up of the three mutually orthogonal vectors that together determine the rotation/orientation of the moving frame with respect to the fixed frame, and it constitutes the 3 × 3 (top-left) submatrix of the 4 × 4 homogeneous transformation matrix.

once  $\mathbf{T}$  is determined, the position vector<sup>7</sup> of the vertex  $H_1 \equiv O_8$  as well as the orientation of the upper platform can be extracted from it. Using these two quantities, the position vector of the center of the upper platform can then easily be calculated, which effectively completes the description of the end-effector pose. Now, it is known from Section 2.2 that  $\mathbf{T}$  contains both active (known) and passive (unknown) joint variables. The passive joint variables can be determined using the leg constraints for the other two limbs, that is,  $B_2M_2H_2$  and  $B_3M_3H_3$ . A two-stage procedure is adopted as discussed below – first determining the passive joint variables  $\theta_1$  and  $\theta_3$  of the lower mechanism in terms of the active joint variables (the values of which are given) and then using the determined values along with the active joint variables to solve for the passive joint variables  $\theta_4$  and  $\theta_5$  of the upper mechanism. The overall transformation matrix  $\mathbf{T}$  can now be fully determined using these values.

### 3.1. Lower parallel (1-RRR 2-SPS) mechanism

The values of  $\theta_2, L_2, L_3$  are given, and the values of the passive joint variables  $\theta_1$  and  $\theta_3$  are required. Now, from the geometry of the manipulator, the following vectors<sup>8</sup> can be written:

$${}^1\mathbf{O}_1\mathbf{B}_2 = [b_2, 0, 0, 1]^T \tag{4}$$

$${}^1\mathbf{O}_1\mathbf{B}_3 = [b_{3x}, 0, b_{3z}, 1]^T \tag{5}$$

$${}^4\mathbf{O}_4\mathbf{M}_2 = [0, 0, \sqrt{3}h_1, 1]^T \tag{6}$$

$${}^4\mathbf{O}_4\mathbf{M}_3 = \left[ \sqrt{3}h_1 \sin \frac{\pi}{3}, 0, \sqrt{3}h_1 \cos \frac{\pi}{3}, 1 \right]^T = \left[ \frac{3h_1}{2}, 0, \frac{\sqrt{3}h_1}{2}, 1 \right]^T \tag{7}$$

Now the vectors in Eqs. (6) and (7) are transformed to frame 1 as:

$${}^1\mathbf{O}_1\mathbf{M}_2 = \mathbf{T}_1 {}^4\mathbf{O}_4\mathbf{M}_2 \tag{8}$$

$${}^1\mathbf{O}_1\mathbf{M}_3 = \mathbf{T}_1 {}^4\mathbf{O}_4\mathbf{M}_3 \tag{9}$$

The leg vectors  ${}^1\mathbf{L}_2$  and  ${}^1\mathbf{L}_3$  are written as:

$${}^1\mathbf{L}_2 = {}^1\mathbf{O}_1\mathbf{M}_2 - {}^1\mathbf{O}_1\mathbf{B}_2 \tag{10}$$

$${}^1\mathbf{L}_3 = {}^1\mathbf{O}_1\mathbf{M}_3 - {}^1\mathbf{O}_1\mathbf{B}_3 \tag{11}$$

Using the given leg lengths:

$${}^1\mathbf{L}_2 \cdot {}^1\mathbf{L}_2 - L_2^2 = 0 \tag{12}$$

$${}^1\mathbf{L}_3 \cdot {}^1\mathbf{L}_3 - L_3^2 = 0 \tag{13}$$

Using Eqs. (4)–(11), the above two equations are written in the following form:

$$p_1c_1 + p_2s_1 + p_3 = 0 \tag{14}$$

$$q_1c_1 + q_2s_1 + q_3c_3 + q_4s_3 + q_5c_1c_3 + q_6s_1s_3 + q_7 = 0 \tag{15}$$

where,

$$\begin{aligned}
 p_1 &= 2\sqrt{3}b_2h_1s_2; & p_2 &= 2L_1b_2; & p_3 &= L_1^2 - L_2^2 + b_2^2 + 3h_1^2 \\
 q_1 &= \sqrt{3}h_1b_{3x}s_2; & q_2 &= 2L_1b_{3x}; & q_3 &= 3h_1b_{3z}; & q_4 &= -3h_1L_1; & q_5 &= -3h_1b_{3x}c_2 \\
 q_6 &= -3h_1b_{3x}; & q_7 &= \sqrt{3}h_1b_{3z}c_2 + L_1^2 - L_3^2 + b_{3x}^2 + b_{3z}^2 + 3h_1^2
 \end{aligned}
 \tag{16}$$

<sup>7</sup>By definition of the homogeneous transformation matrix, this is the  $3 \times 1$  vector formed using the components in the first three rows of the fourth column of  $\mathbf{T}$ .

<sup>8</sup>Where the fourth coordinate represents the homogeneous coordinate.

Since Eq. (14) is only a function of  $\theta_1$ , it can be solved by using half-angle substitution to get two solutions (corresponding to  $\pm$ ) for  $\theta_1$  as:

$$\theta_{1,2} = 2 \tan^{-1} \left( \frac{p_2 \pm \sqrt{p_1^2 + p_2^2 - p_3^2}}{p_1 - p_3} \right) \tag{17}$$

Here,  $\tan^{-1}$  gives a solution in the range  $\left(-\frac{\pi}{2}, \frac{\pi}{2}\right)$ . Substituting the obtained value of  $\theta_1$  in Eq. (15) gives the following equation:

$$k_1 c_3 + k_2 s_3 + k_3 = 0 \tag{18}$$

where,

$$k_1 = q_5 c_1 + q_3; \quad k_2 = q_6 s_1 + q_4; \quad k_3 = q_1 c_1 + q_2 s_1 + q_7 \tag{19}$$

The solution for  $\theta_3$  using Eq. (18) is given as:

$$\theta_{3,2} = 2 \tan^{-1} \left( \frac{k_2 \pm \sqrt{k_1^2 + k_2^2 - k_3^2}}{k_1 - k_3} \right) \tag{20}$$

In total,  $2 \times 2 = 4$  solution sets of  $\theta_1$  and  $\theta_3$  are obtained. For each solution set, the transformation matrix  $T_1$  can be fully determined, which completes the forward kinematics of the lower parallel mechanism.

**3.2. Upper parallel 3-UPU TPM mechanism**

For analyzing the 3-UPU mechanism, a similar procedure is adopted as done for the lower parallel mechanism. Here, the values of  $L_4, L_5, L_6$  are given, and the values of the passive joint variables  $\theta_4$  and  $\theta_5$  are determined. The components of the relevant vectors obtained from the geometry of the manipulator are given below:

$${}^4_u \mathbf{O}_4 \mathbf{M}_2 = \left[ \sqrt{3}h_1 \cos \frac{\pi}{6}, 0, \sqrt{3}h_1 \sin \frac{\pi}{6}, 1 \right]^T = \left[ \frac{3h_1}{2}, 0, \frac{\sqrt{3}h_1}{2}, 1 \right]^T \tag{21}$$

$${}^4_u \mathbf{O}_4 \mathbf{M}_3 = \left[ \sqrt{3}h_1 \cos \frac{\pi}{6}, 0, -\sqrt{3}h_1 \sin \frac{\pi}{6}, 1 \right]^T = \left[ \frac{3h_1}{2}, 0, -\frac{\sqrt{3}h_1}{2}, 1 \right]^T \tag{22}$$

$${}^8 \mathbf{O}_8 \mathbf{H}_2 = \left[ \sqrt{3}h_2 \cos \frac{\pi}{6}, 0, \sqrt{3}h_2 \sin \frac{\pi}{6}, 1 \right]^T = \left[ \frac{3h_2}{2}, 0, \frac{\sqrt{3}h_2}{2}, 1 \right]^T \tag{23}$$

$${}^8 \mathbf{O}_8 \mathbf{H}_3 = \left[ \sqrt{3}h_2 \cos \frac{\pi}{6}, 0, -\sqrt{3}h_2 \sin \frac{\pi}{6}, 1 \right]^T = \left[ \frac{3h_2}{2}, 0, -\frac{\sqrt{3}h_2}{2}, 1 \right]^T \tag{24}$$

Now, the vectors in Eqs. (23) and (24) can be transformed to frame  $4_u$  as:

$${}^4_u \mathbf{O}_4 \mathbf{H}_2 = T_2 {}^8 \mathbf{O}_8 \mathbf{H}_2 \tag{25}$$

$${}^4_u \mathbf{O}_4 \mathbf{H}_3 = T_2 {}^8 \mathbf{O}_8 \mathbf{H}_3 \tag{26}$$

The leg vectors  ${}^4_u \mathbf{L}_5$  and  ${}^4_u \mathbf{L}_6$  can be written as:

$${}^4_u \mathbf{L}_5 = {}^4_u \mathbf{O}_4 \mathbf{H}_2 - {}^4_u \mathbf{O}_4 \mathbf{M}_2 \tag{27}$$

$${}^4_u \mathbf{L}_6 = {}^4_u \mathbf{O}_4 \mathbf{H}_3 - {}^4_u \mathbf{O}_4 \mathbf{M}_3 \tag{28}$$



The leg length constraint equations are:

$${}^4_u\mathbf{L}_5 \cdot {}^4_u\mathbf{L}_5 - L_5^2 = 0 \tag{29}$$

$${}^4_u\mathbf{L}_6 \cdot {}^4_u\mathbf{L}_6 - L_6^2 = 0 \tag{30}$$

Using Eqs. (21)–(28) in Eqs. (29) and (30), then adding Eqs. (29) and (30), and subtracting Eqs. (30) from (29), yields the following two equations:

$$f_1s_5 + f_2 = 0 \tag{31}$$

$$g_1c_4c_5 + g_2 = 0 \tag{32}$$

where

$$f_1 = -2\sqrt{3}L_4(h_1 - h_2); \quad f_2 = L_6^2 - L_5^2 \tag{33}$$

$$g_1 = -6L_4(h_1 - h_2); \quad g_2 = 2L_4^2 - L_5^2 - L_6^2 + 6(h_1 - h_2)^2$$

Since Eq. (31) is only a function of  $\theta_5$ , the two solutions are written as:

$$\theta_{5,1,2} = \sin^{-1} \left( -\frac{f_2}{f_1} \right) \tag{34}$$

Now substituting the value of  $\theta_5$  obtained in Eq. (32), the following equation is obtained:

$$w_1c_4 + w_2 = 0 \tag{35}$$

where,

$$w_1 = g_1c_5; \quad w_2 = g_2 \tag{36}$$

The two solutions for  $\theta_4$  from the above equation are written as:

$$\theta_{4,1,2} = \cos^{-1} \left( -\frac{w_2}{w_1} \right) \tag{37}$$

In total,  $2 \times 2 = 4$  solution sets of  $\theta_4$  and  $\theta_5$  are obtained. For each solution set, the transformation matrix  $\mathbf{T}_2$  can be fully determined, which completes the forward kinematics of the upper parallel mechanism. However, these four distinct joint space solution sets for the upper parallel mechanism result in only two distinct poses, that is, only two distinct task space configurations. The reason for this lies in the interdependence of the four joint space solution sets, that is, say the first solution set is  $\{\theta_4 = \beta_4, \theta_5 = \beta_5\}$ , then the other three solution sets are given as  $\{(\beta_4 - \pi), (\pi - \beta_5)\}, \{-\beta_4, \beta_5\}, \{(\pi - \beta_4), (\pi - \beta_5)\}$ . So rotating about the two revolute axes of the universal joint  $U_1$  following the first solution set values for  $\theta_4$  and  $\theta_5$ , and then again following the second solution set values leads to the same final configuration.

Similarly, the third and the fourth solution sets lead to the same final configuration, but it is different from the one attained by the first two solution sets. Therefore, only two distinct task space configurations are obtained, as would be numerically illustrated later in Section 5.2.1 as well. This fact can also be directly deduced easily by substituting the solution sets into the symbolic form of  $\mathbf{T}_2$  and observing that there are indeed only two distinct  $\mathbf{T}_2$  matrices, and hence only two distinct poses. Moreover, the two obtained task space configurations are related to each other – if the upper mechanism of one of the configurations is reflected in the mid-plane, the other configuration is obtained. In other words, both task space configurations are just the reflection of the upper mechanism in the mid-plane, with the lower mechanism configuration being the same.

### 3.3. Determining the overall transformation matrix

Overall,  $4 \times 4 = 16$  distinct solution sets of  $(\theta_1, \theta_3, \theta_4, \theta_5)$  quadruplet of passive variables are obtained that correspond to a total of 16 possible direct kinematic solutions in joint space for the complete hybrid manipulator. However, for the above-mentioned reason in Section 3.2, there are only  $4 \times 2 = 8$  direct kinematic solutions in task space.

Having determined all the passive variables and consequently evaluating the matrices  $T_1$  and  $T_2$ , the overall transformation matrix  $T_2$  can be determined using Eq. (2). Further, the position vector of vertex  $H_1$ , as well as the orientation of the upper platform, can be extracted from it, which can be used to get the position vector of any other point (including the center) of the upper platform. Therefore, this completes the forward kinematic analysis of the proposed hybrid manipulator.

**4. Closed-form inverse position analysis**

The most crucial part in the control of any manipulator is the efficient and accurate calculation of the inverse kinematics of the manipulator, in which the required joint motions are to be found from the given pose of the end-effector. In the context of the present hybrid manipulator, given the pose of the upper platform H [i.e., given the overall transformation matrix  $T$  of Eq. (2)], the active joint variables  $\theta_2, L_2, L_3, L_4, L_5, L_6$  need to be determined. Owing to the particular structure of the hybrid manipulator, the orientation part of  $T$  contains the active and the passive variables of *only* the lower parallel mechanism; this facilitates the decoupling of the inverse kinematic analysis into two separate parts: one for the lower mechanism and the other for the upper mechanism, as discussed below. Now, let the given numerical overall transformation matrix be  $T_{num}$ .

**4.1. Lower parallel (1-RRR 2-SPS) mechanism**

Let the orientation part of  $T_{num}$  be:

$$Q_{num} = \begin{bmatrix} q_{11} & q_{12} & q_{13} \\ q_{21} & q_{22} & q_{23} \\ q_{31} & q_{32} & q_{33} \end{bmatrix} \tag{38}$$

From the components of  $T$  described in symbolic form in Section 2.2, the components of the orientation part are extracted to get the orientation matrix  $Q$  in symbolic form, which can then be compared with the given numerical orientation matrix  $Q_{num}$  to solve for the active and the passive variables of the lower mechanism. So using the fact that  $Q \equiv Q_{num}$ , and comparing their (3,1), (3,2), and (3,3) elements, the following three equations are obtained:

$$q_{31} = -\frac{s_2 c_3}{2} - \frac{\sqrt{3} c_2}{2} \tag{39}$$

$$q_{32} = s_2 s_3 \tag{40}$$

$$q_{33} = \frac{\sqrt{3} s_2 c_3}{2} - \frac{c_2}{2} \tag{41}$$

where the RHS<sup>9</sup> is known, while the LHS is unknown. Multiplying Eq. (39) by  $\sqrt{3}$  and adding it to Eq. (41), followed by suitable manipulation gives

$$c_2 = -\frac{1}{2} (\sqrt{3} q_{31} + q_{33}) \tag{42}$$

$$s_2 c_3 = -\frac{1}{2} (q_{31} - \sqrt{3} q_{33}) \tag{43}$$

Now, dividing the RHS of Eq. (40) by LHS of Eq. (43) (provided  $s_2 \neq 0$ ) gives

$$\theta_{3,1,2} = \arctan \left( -\frac{2 q_{32}}{(q_{31} - \sqrt{3} q_{33})} \right) \tag{44}$$

<sup>9</sup>RHS and LHS refer to the right-hand side and the left-hand side of the equation under consideration, respectively.

Therefore, two solutions<sup>10</sup> (having a difference of  $\pi$ ) are obtained for  $\theta_3$ . In order to get  $\theta_2$ , the obtained  $\theta_3$  value is substituted in Eq. (40) to get:

$$s_2 = \frac{q_{32}}{s_3} \tag{45}$$

From Eqs. (42) and (45), the value of  $\theta_2$  can be obtained:

$$\theta_2 = \text{Atan2}(s_2, c_2) \tag{46}$$

Now, in order to get  $\theta_1$ , the (1,2) and (2,2) elements of  $\mathbf{Q}$  and  $\mathbf{Q}_{\text{num}}$  are compared and the calculated values of  $\theta_2$  and  $\theta_3$  are substituted to get the following two equations in  $s_1$  and  $c_1$ :

$$q_{12} = s_1 c_3 - c_1 c_2 s_3 \tag{47}$$

$$q_{22} = -c_1 c_3 - s_1 c_2 s_3 \tag{48}$$

Eliminating  $c_1$  using Eqs. (47) and (48), an equation in  $s_1$  of the following form is obtained:

$$a_1 s_1 + a_2 = 0 \implies s_1 = -\frac{a_2}{a_1} \tag{49}$$

where the coefficients are in terms of the known quantities,

$$a_1 = c_3^2 + c_2^2 s_3^2; \quad a_2 = -c_3 q_{12} + c_2 s_3 q_{22} \tag{50}$$

Substituting back  $s_1$  in Eq. (47), an equation in  $c_1$  is obtained:

$$b_1 c_1 + b_2 = 0 \implies c_1 = -\frac{b_2}{b_1} \tag{51}$$

where the coefficients are in terms of the known quantities,

$$b_1 = c_3^2 + c_2^2 s_3^2; \quad b_2 = c_2 s_3 q_{12} + c_3 q_{22} \tag{52}$$

From Eqs. (49) and (51), the value of  $\theta_1$  can be obtained:

$$\theta_1 = \text{Atan2}(s_1, c_1) \tag{53}$$

Finally, overall, two solutions are obtained, since for each of the two possible  $\theta_3$  values, unique solutions for  $\theta_1$  and  $\theta_2$  exist. Also, now the values of  $\theta_1, \theta_2$ , and  $\theta_3$  can be substituted into Eqs. (10) and (11) to obtain the leg length vectors, and then  $L_2$  and  $L_3$  can be calculated using Eqs. (12) and (13), respectively, as:

$$L_2 = \sqrt{{}^1\mathbf{L}_2 \cdot {}^1\mathbf{L}_2} \tag{54}$$

$$L_3 = \sqrt{{}^1\mathbf{L}_3 \cdot {}^1\mathbf{L}_3} \tag{55}$$

It is to be noted that, for the reasons stated earlier<sup>6</sup> on Page 6, the limb lengths  $L_2$  and  $L_3$  are only taken to be positive.<sup>11</sup>

This completes the inverse kinematics for the lower parallel mechanism since there are now the values for  $\theta_1, \theta_2, \theta_3, L_2$  and  $L_3$ . Further, the numeric  $\mathbf{T}_{1\text{num}}$  matrix can be obtained by substituting all these values in the symbolic form of  $\mathbf{T}_1$ .

#### 4.2. Upper parallel 3-UPU TPM mechanism

Now, since the inverse kinematics is solved for the lower parallel mechanism, we can decouple the overall numeric transformation matrix  $\mathbf{T}_{\text{num}}$  using Eq. (2) and get the transformation matrix  $\mathbf{T}_{2\text{num}}$  having

<sup>10</sup>Each of the  $\theta$ 's can take any value from  $[-\pi, \pi]$ , and thus, the second solution as tan has a period of  $\pi$ .

<sup>11</sup>Moreover,  $L_2$  and  $L_3$  can only be negative together at the same time, that is, it cannot be that one of them is negative and the other is positive. So for each of the two values of  $\theta_3$ , two solutions are seen where one has positive  $L_2$  and  $L_3$ , while the other has negative  $L_2$  and  $L_3$ . Thus, four solutions exist for the inverse kinematics of the lower mechanism. However, as only the positive  $L_2$  and  $L_3$  solutions are considered, it results in just two solutions of the total 4.

the following form as:

$$\mathbf{T}_{2_{\text{num}}} = (\mathbf{T}_{1_{\text{num}}} \mathbf{C}_u^l)^{-1} \mathbf{T}_{\text{num}} = \begin{bmatrix} 1 & 0 & 0 & r_x \\ 0 & 1 & 0 & r_y \\ 0 & 0 & 1 & r_z \\ 0 & 0 & 0 & 1 \end{bmatrix} \tag{56}$$

Moreover, the symbolic form of  $\mathbf{T}_2$  matrix found out using the D-H Table II is

$$\mathbf{T}_2 = \begin{bmatrix} 1 & 0 & 0 & L_4 c_4 c_5 \\ 0 & 1 & 0 & L_4 s_4 c_5 \\ 0 & 0 & 1 & L_4 s_5 \\ 0 & 0 & 0 & 1 \end{bmatrix} \tag{57}$$

Thus, exploiting the fact that  $\mathbf{T}_2 \equiv \mathbf{T}_{2_{\text{num}}}$ , and comparing their (1,4), (2,4) and (3,4) elements, the following three equations are seen:

$$r_x = L_4 c_4 c_5 \tag{58}$$

$$r_y = L_4 s_4 c_5 \tag{59}$$

$$r_z = L_4 s_5 \tag{60}$$

Squaring and adding Eqs. (58), (59) and (60),  $L_4$  is obtained as:

$$L_4 = \sqrt{r_x^2 + r_y^2 + r_z^2} \tag{61}$$

Also, dividing Eqs. (59) and (58), two solutions for  $\theta_4$  are obtained as:

$$\theta_{4,1,2} = \arctan\left(\frac{r_y}{r_x}\right) \tag{62}$$

Now, using the values of  $L_4$  and  $\theta_4$  in Eqs. (59) and (60),  $s_5$  and  $c_5$ , and therefore,  $\theta_5$  are found out as:

$$s_5 = \frac{r_z}{L_4} \tag{63}$$

$$c_5 = \frac{r_y}{L_4 s_4} \tag{64}$$

$$\implies \theta_5 = \text{Atan2}(s_5, c_5) \tag{65}$$

So, again, there are overall two solutions, since for each of the two possible  $\theta_4$  values, there exist unique solutions for  $L_4$  and  $\theta_5$ . However, the two solution sets of  $\theta_4$  and  $\theta_5$  are of the form  $\{\beta_4, \beta_5\}$  and  $\{(\beta_4 - \pi), (\pi - \beta_5)\}$ , which again lead to same task space configuration, for reasons mentioned earlier in Section 3.2. Thus, only one distinct task space configuration exists corresponding to the two inverse kinematic solutions of the upper parallel mechanism.

Now, the values of  $\theta_4$ ,  $\theta_5$ , and  $L_4$  can be substituted into Eqs. (27) and (28) to obtain the leg length vectors, and then  $L_5$  and  $L_6$  can be calculated using Eqs. (29) and (30), respectively, as:

$$L_5 = \sqrt{{}^4u\mathbf{L}_5 \cdot {}^4u\mathbf{L}_5} \tag{66}$$

$$L_6 = \sqrt{{}^4u\mathbf{L}_6 \cdot {}^4u\mathbf{L}_6} \tag{67}$$

It is to be noted that, here also, for the reasons stated earlier<sup>6</sup> on Page 6, the limb lengths  $L_4$ ,  $L_5$ , and  $L_6$  are only taken to be positive.<sup>12</sup>

<sup>12</sup>Again, for each of the two values of  $\theta_4$ , two solutions are seen where one of them has positive  $L_4$ ,  $L_5$  and  $L_6$ , while the other has negative  $L_4$ ,  $L_5$  and  $L_6$ . Thus, there are four solutions in total for the inverse kinematics of the upper mechanism. However, only the positive  $L_4$ ,  $L_5$ , and  $L_6$  solutions are considered, leaving just the two solutions of the total 4.

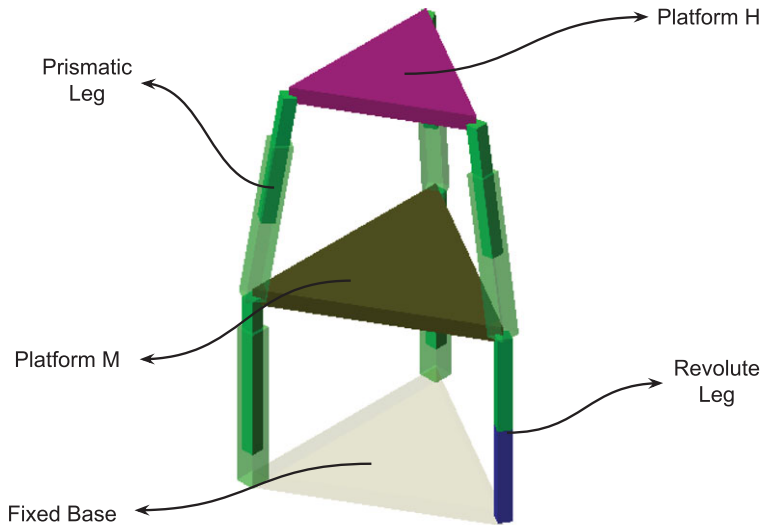


**Figure 3.** Simulated 3D model of the hybrid manipulator in Simscape Multibody (in Simscape Multibody models, joints are not displayed in the final simulated 3D model).

Finally,  $2 \times 2 = 4$  possible inverse kinematic solutions are obtained for the complete hybrid manipulator in joint space. However, only  $2 \times 1 = 2$  inverse kinematic solutions are seen with distinct task space configurations. This fact will also be numerically illustrated later in Section 5.2.2.

Thus, this completes the inverse kinematic analysis of the hybrid manipulator as all the actuated joint variables  $\theta_2, L_2, L_3, L_4, L_5, L_6$  have been obtained from the given pose of the end-effector.

## 5. 3D modeling, numerical verification, and simulation

### 5.1. Model

In the literature, different simulation environments have been developed and used, some of which, such as the RoboSim and RoboAnalyzer<sup>®</sup>, are specialized in robotics. In contrast, others are generic 3D simulation software, such as Adams<sup>™</sup>, MapleSim<sup>™</sup>, and Simscape<sup>™</sup> Multibody<sup>™</sup> (earlier SimMechanics<sup>™</sup>). In this paper, the proposed hybrid manipulator is modeled and simulated using Simscape Multibody, which is based on Simulink<sup>®</sup> and MATLAB<sup>®</sup>. The advantage of using Simscape Multibody is that sensing various signals, including joint movements and displacements, torques, and forces, becomes much more accessible.

The 3D model of the hybrid manipulator is shown in Fig. 3, while Fig. 4(a) shows the complete hybrid manipulator block diagram built in Simscape Multibody. The whole model is made up of five parts: base, lower parallel mechanism, platform M, upper parallel mechanism, and platform H, where the lower mechanism and upper mechanism models, as shown in Fig. 4(b) and (c), respectively, have been built in accordance with the geometry and structure presented in Section 2.1.

### 5.2. Numerical example

Consider the following numerical example with the chosen design parameters:

$$\begin{aligned}
 b_2 &= 40\sqrt{3} \text{ cm} = 69.28 \text{ cm}; & b_{3_x} &= 20\sqrt{3} \text{ cm} = 34.64 \text{ cm}; & b_{3_z} &= 60 \text{ cm} \\
 h_1 &= 40 \text{ cm}; & h_2 &= 30 \text{ cm}; & L_1 &= 60 \text{ cm}
 \end{aligned}
 \tag{68}$$

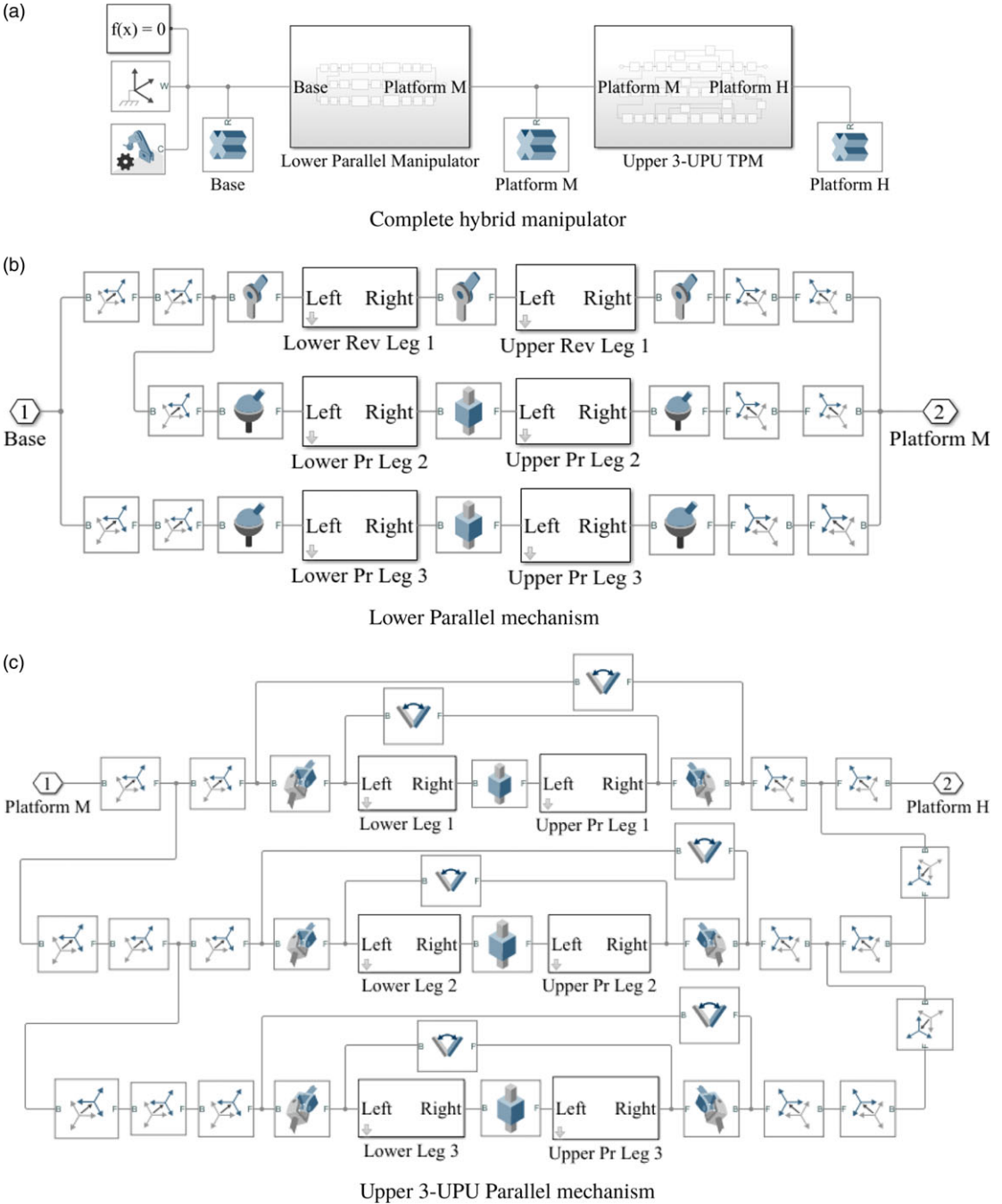


**Figure 4.** Model of the proposed hybrid manipulator built in Simscape Multibody.

5.2.1. Forward kinematics

The following active joint variable values are noted:

$$\begin{aligned}
 \theta_2 &= \frac{\pi}{3} \text{ rad}; & L_2 &= 49 \text{ cm}; & L_3 &= 81 \text{ cm} \\
 L_4 &= 60 \text{ cm}; & L_5 &= 59 \text{ cm}; & L_6 &= 70 \text{ cm}
 \end{aligned}
 \tag{69}$$

**Table III.** All 16 solutions for the DK of the hybrid manipulator, with each pair of it corresponding to a single configuration.

<i>i</i>	Lower		Upper	
	$\theta_1$ (rad)	$\theta_3$ (rad)	$\theta_4$ (rad)	$\theta_5$ (rad)
1	-2.7628	-2.7336	1.7935	0.7515
2	-2.7628	-2.7336	-1.3481	2.3901
3	-2.7628	-2.7336	-1.7935	0.7515
4	-2.7628	-2.7336	1.3481	2.3901
5	-2.7628	1.5209	1.7935	0.7515
6	-2.7628	1.5209	-1.3481	2.3901
7	-2.7628	1.5209	-1.7935	0.7515
8	-2.7628	1.5209	1.3481	2.3901
9	-1.9496	-2.5702	1.7935	0.7515
10	-1.9496	-2.5702	-1.3481	2.3901
11	-1.9496	-2.5702	-1.7935	0.7515
12	-1.9496	-2.5702	1.3481	2.3901
13	-1.9496	1.6808	1.7935	0.7515
14	-1.9496	1.6808	-1.3481	2.3901
15	-1.9496	1.6808	-1.7935	0.7515
16	-1.9496	1.6808	1.3481	2.3901

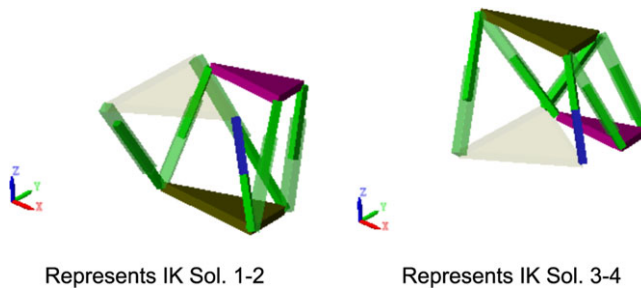


**Figure 5.** Eight distinct task space solutions, with each representing a pair of joint space solutions in Table III.

Solving Eq. (14), two solutions are obtained as  $\theta_{1_1} = -2.7628$  rad and  $\theta_{1_2} = -1.9496$  rad. Further, solving Eq. (18) with  $\theta_{1_1}$  as the solution leads to  $\theta_{3_1}^1 = -2.7336$  rad and  $\theta_{3_2}^1 = 1.5209$  rad, while with  $\theta_{1_2}$  as the solution, it gives  $\theta_{3_1}^2 = -2.5702$  rad and  $\theta_{3_2}^2 = 1.6808$  rad.

For  $\theta_5$ , Eq. (31) is solved to get  $\theta_{5_1} = 0.7515$  rad and  $\theta_{5_2} = 2.3901$  rad. Solving Eq. (35) with  $\theta_{5_1}$  as the solution, it gives  $\theta_{4_1}^1 = 1.7935$  rad and  $\theta_{4_2}^1 = -1.7935$  rad, while with  $\theta_{5_2}$  as the solution, it gives  $\theta_{4_1}^2 = 1.3481$  rad and  $\theta_{4_2}^2 = -1.3481$  rad. As can be seen, the solutions for  $\theta_4$  are symmetric about the mid-platform M. All the 16 possible joint space solutions to the forward kinematics have been listed in Table III. Also, as was stated earlier in Section 3.2, on calculating the overall transformation matrix **T** for each of the 16 solutions, only 8 distinct task space configurations are obtained, which have been depicted in Fig. 5.

5.2.2. Inverse kinematics

Consider the 4th solution  $\{\theta_{1_1} = -2.7628$  rad,  $\theta_{3_1}^1 = -2.7336$  rad,  $\theta_{5_2} = 2.3901$  rad,  $\theta_{4_1}^2 = 1.3481$  rad $\}$  of the 16 total solutions for the direct kinematics presented above. For this solution, the numerical overall

**Table IV.** All four solutions to the inverse kinematics of the hybrid manipulator, with each pair of it corresponding to a single configuration.

i	Lower					Upper				
	$\theta_1$ (rad)	$\theta_2$ (rad)	$\theta_3$ (rad)	$L_2$ (cm)	$L_3$ (cm)	$\theta_4$ (rad)	$\theta_5$ (rad)	$L_4$ (cm)	$L_5$ (cm)	$L_6$ (cm)
1	0.3788	-1.0472	0.4080	92.467	62.623	1.3642	-0.0039	68.855	67.986	67.916
2	0.3788	-1.0472	0.4080	92.467	62.623	-1.7774	3.1455	68.855	67.986	67.916
3	-2.7628	1.0472	-2.7336	49.0	81.0	1.3481	2.3901	60.0	59.0	70.0
4	-2.7628	1.0472	-2.7336	49.0	81.0	-1.7935	0.7515	60.0	59.0	70.0

transformation matrix  $T_{num}$  is

$$T_{num} = \begin{bmatrix} 0.9834 & 0.1551 & -0.0941 & 2.181 \\ 0.1778 & -0.9262 & 0.3324 & -4.249 \\ -0.0355 & -0.3436 & -0.9384 & -23.403 \\ 0 & 0 & 0 & 1 \end{bmatrix} \tag{70}$$

Given this matrix, the inverse kinematics involves solving for the joint variables. So, solving for  $\theta_3$ , two solutions are seen as  $\theta_{3_1} = 0.4080$  rad and  $\theta_{3_2} = -2.7336$  rad. Corresponding to  $\theta_{3_1}$ ,  $\theta_2^1 = -1.0472$  rad and  $\theta_1^1 = 0.3788$  rad are seen, while for  $\theta_{3_2}$ ,  $\theta_2^2 = 1.0472$  rad and  $\theta_1^2 = -2.7628$  rad are seen. Thus, two solutions are obtained here for lower parallel mechanism. Now, for instance, for the solution, which is  $\{\theta_{3_1} = 0.4080$  rad,  $\theta_2^1 = -1.0472$  rad,  $\theta_1^1 = 0.3788$  rad $\}$ , the decoupled  $T_{2num}$  matrix is obtained as:

$$T_{2num} = \begin{bmatrix} 1 & 0 & 0 & 14.124 \\ 0 & 1 & 0 & 67.390 \\ 0 & 0 & 1 & -0.274 \\ 0 & 0 & 0 & 1 \end{bmatrix} \tag{71}$$

From this,  $L_4$  is obtained as 68.855 cm. Further, the two solutions are obtained as  $\theta_{4_1} = 1.3642$  rad and  $\theta_{4_2} = -1.7774$  rad, and corresponding to them  $\theta_5^1 = -0.0039$  rad and  $\theta_5^2 = 3.1455$  rad are seen, respectively. Therefore, again, there are two solutions for the upper parallel mechanism for any given solution to the lower one. Hence, four possible joint space solutions are obtained to the inverse kinematics problem of the complete hybrid manipulator and are listed in Table IV.<sup>13</sup> Also, as was stated earlier in Section 4.2, there are only two distinct configurations, as depicted in Fig. 6.

**5.3. Simulation example: translation in a specific direction in a plane parallel to an oblique plane**

Consider the following example in which a planar translation of the upper platform is desired along a specified translational direction while maintaining some constant orientation with respect to the base. As described in Section 1, four parameters can be specified, of which the offset distance and the required orientation of the mid-platform are embedded in the given  $T_{1num}$  matrix:

$$T_{1num} = \begin{bmatrix} -0.125 & 0.6495 & 0.75 & 30.0 \\ -0.6495 & -0.625 & 0.4330 & -51.961 \\ 0.75 & -0.4330 & 0.5 & 0 \\ 0 & 0 & 0 & 1 \end{bmatrix} \tag{72}$$

<sup>13</sup>It is to be noted that the forward kinematic solution from Table III, from which we started, is obtained back in the form of the inverse kinematic solution here. This also cross-verifies both the DK and IK analyses.



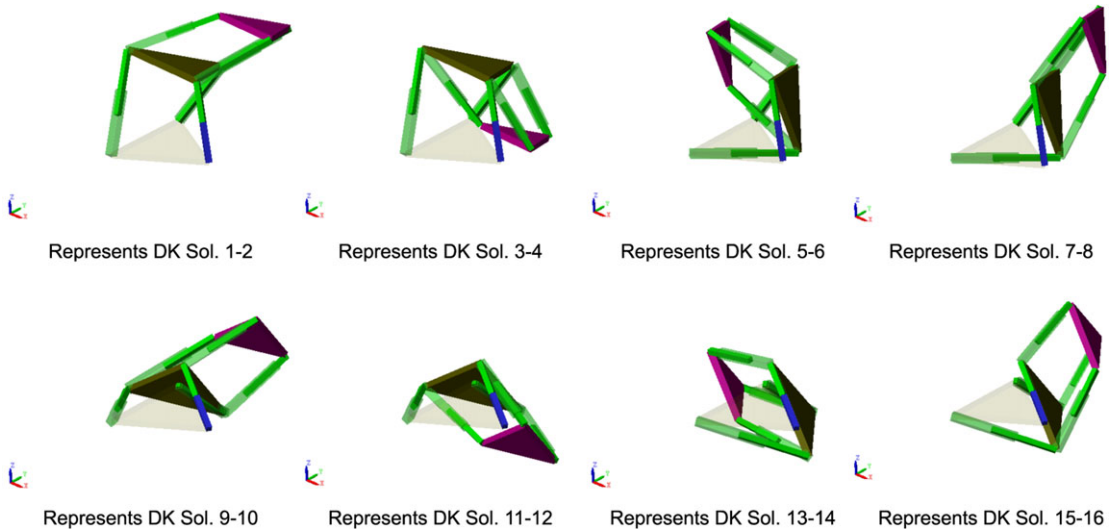


Figure 6. Two distinct configurations, with each representing a pair of solutions in Table IV.

The desired perpendicular distance is 50 cm. The translational motion is expected to be along the  $X_8 \equiv X_{4u}$  axis, such that it first translates 50 cm along  $-X_8$  axis, and then from that point onward it translates 100 cm along the  $+X_8$  axis, effectively ending the motion at a displacement of 50 cm along  $+X_8$  axis. Furthermore, the same design parameters were used as mentioned in Eq. (68) in Section 5.2.

For the simulation, inverse kinematics was performed on the desired motion to get the actuated joint values, which were then fed to the model. The resulting simulation is presented in Fig. 7, showing the three stages of motions. Also, the simulated translational motion measured using the Transform Sensor Block in Simscape Multibody is shown in Fig. 8, and it clearly matches the desired motion.

During the simulation, the joint limits were added appropriately to only allow for feasible motions.

### 6. Singularity analysis

Singularity analysis of serial and parallel manipulators has been quite extensively studied in the literature, and different types of singularities have been identified [6]. In the following subsections, the singularity analysis of the proposed hybrid manipulator is presented, and all of its singularities in the joint space of active joints are determined. Consider the following vectors defined as:

$$\Theta = [\theta_2(t), L_2(t), L_3(t), L_4(t), L_5(t), L_6(t)]^T : \text{vector of all active joint variables}$$

$$\Phi = [\theta_1(t), \theta_3(t), \theta_4(t), \theta_5(t)]^T : \text{vector of all passive joint variables in the formulation, i.e., along limb } B_1M_1H_1$$

$$q = [\theta_1(t), \theta_2(t), \theta_3(t), \theta_4(t), \theta_5(t), L_4(t)]^T : \text{vector of all the joint variables (active + passive) in the formulation, i.e., along limb } B_1M_1H_1$$

$$\$ = [\omega_x, \omega_y, \omega_z, v_x, v_y, v_z]^T : \text{the twist vector of the end-effector (platform H)}$$

First, the singularities occurring due to the parallel structure of the hybrid manipulator are determined, which we loosely call the “parallel singularities.” Differentiating the closed-loop constraint equations (12), (13), (29), and (30) with respect to time, and also introducing two dummy equations:  $\dot{\theta}_2(t) = \dot{\theta}_2(t)$

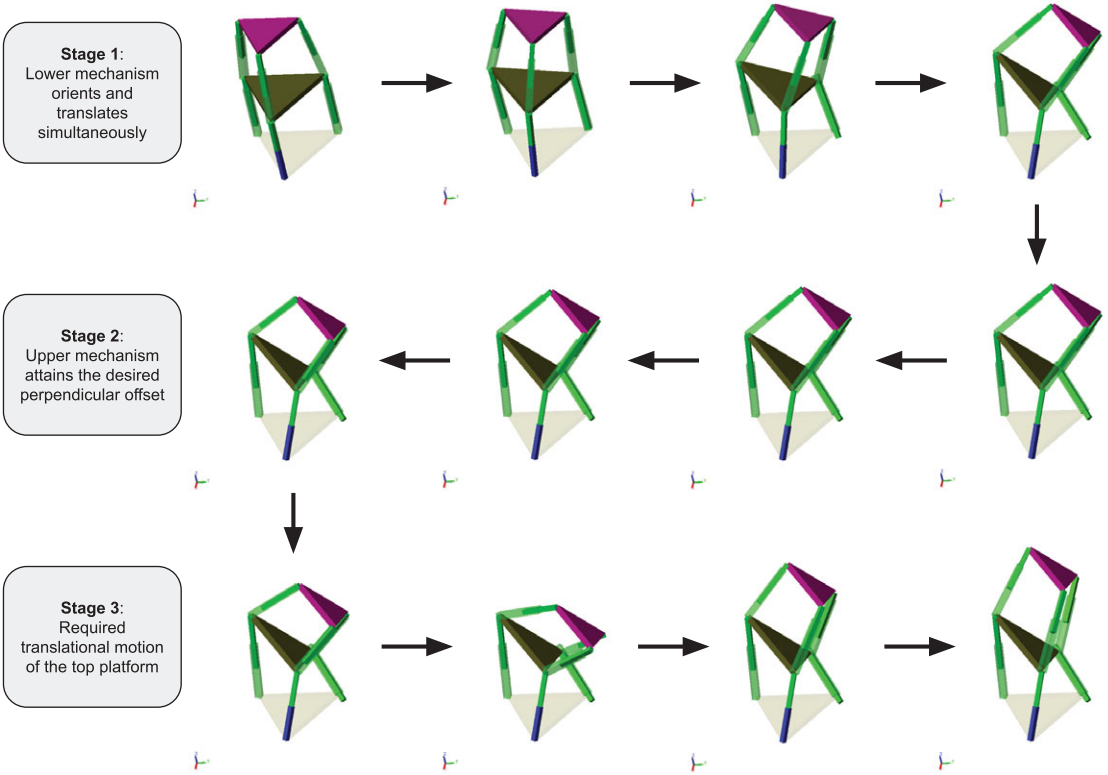


Figure 7. Simulation of the numerical example, showing the three different stages of motion.

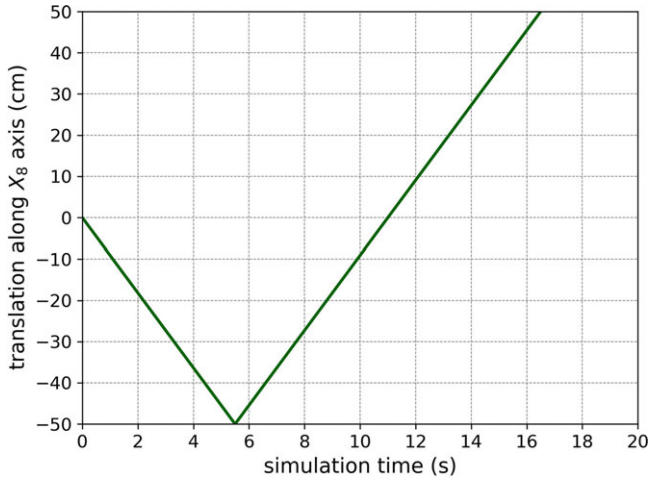


Figure 8. Simulated translational motion.

and  $\dot{L}_4(t) = \dot{L}_4(t)$ , which are trivially satisfied, a convenient and compact matrix form for the six equations is as follows:

$$\mathbf{D} \dot{\Theta}(t) = \mathbf{J}_p \dot{q}(t). \tag{73}$$

Here,  $\mathbf{D} = \mathbf{D}(\Theta(t))$  is a diagonal matrix with the diagonal as  $[1, L_2(t), L_3(t), 1, L_5(t), L_6(t)]$ , and  $\mathbf{J}_p = \mathbf{J}_p(q(t))$  is a  $6 \times 6$  jacobian matrix having the following form (details in Section A.2):

$$\mathbf{J}_p = \begin{bmatrix} 0 & 1 & 0 & 0 & 0 & 0 \\ j_{p21} & j_{p22} & 0 & 0 & 0 & 0 \\ j_{p31} & j_{p32} & j_{p33} & 0 & 0 & 0 \\ 0 & 0 & 0 & 0 & 0 & 1 \\ 0 & 0 & 0 & j_{p54} & j_{p55} & j_{p56} \\ 0 & 0 & 0 & j_{p64} & j_{p65} & j_{p66} \end{bmatrix} \tag{74}$$

It is to be noted that the  $\mathbf{J}_p$  matrix as defined here is closely related to the  $\mathbf{K}^*$  matrix definition given by Ghosal [35] in their analysis of the gain singularities. More specifically,  $\det(\mathbf{J}_p) = \det(\mathbf{K}^*)$ , and thus in accordance with [35],  $\det(\mathbf{J}_p) = 0$  gives Type A (gain) singularity.

**6.1. Type A singularity: DOF-gain singularity**

For the gain singularity to occur,  $\det(\mathbf{J}_p) = 0$  should hold. From Eq. (74), it is known that:

$$\det(\mathbf{J}_p) = j_{p21} j_{p33} (j_{p64} j_{p55} - j_{p54} j_{p65}) = 0 \tag{75}$$

So, from Eq. (75), the following different cases are seen for the gain singularity to occur:

**Case 1:**  $j_{p21} = 0$

Consider

$$j_{p21} = b_2 (L_1 \cos(\theta_1) - \sqrt{3} h_1 \sin(\theta_1) \sin(\theta_2)) = 0 \tag{76}$$

Here,  $b_2 = 0$  is a design singularity, which, however, seems practically infeasible. Now, from Eqs. (76) and (14), there are two equations in  $\theta_1, \theta_2$ , and  $L_2$ :

$$w_1 c_1 + w_2 s_1 s_2 = 0 \tag{77}$$

$$e_1 s_1 + e_2 c_1 s_2 + e_3 = L_2^2 \tag{78}$$

where the coefficients are in terms of the known quantities,

$$w_1 = L_1; \quad w_2 = -\sqrt{3} h_1 \tag{79}$$

$$e_1 = 2L_1 b_2; \quad e_2 = 2\sqrt{3} b_2 h_1; \quad e_3 = L_1^2 + b_2^2 + 3h_1^2$$

Solving Eq. (77) to get two solutions (with a difference of  $\pi$ ) for  $\theta_1$ :

$$\theta_1 = -\arctan\left(\frac{w_1}{w_2 \sin \theta_2}\right) \tag{80}$$

Substituting each value of  $\theta_1$  in Eq. (78), two separate implicit equations are obtained for the two branches of the singularity curve in  $\theta_2$ - $L_2$  plane. For the numerical example presented earlier in Section 5.2, the two branches of the singularity curve are depicted in Fig. 9.

**Case 2:**  $j_{p33} = 0$

$$j_{p33} = -\frac{3}{2} h_1 ((s_1 b_{3x} + L_1) c_3 + (b_{3z} s_2 - b_{3x} c_1 c_2) s_3) = 0 \tag{81}$$

Here, again,  $h_1 = 0$  is a design singularity, which is not feasible practically. Again Eq. (14)  $\equiv f(\theta_1, \theta_2, L_2)$  is used to get two solutions for  $\theta_1 \equiv f(\theta_2, L_2)$ . Substituting  $\theta_1$  back in Eq. (81)  $\equiv f(\theta_1, \theta_2, \theta_3)$ , there are now two solutions for  $\theta_3 \equiv f(\theta_2, L_2)$ . Finally, putting the values of  $\theta_1$  and  $\theta_3$  into Eq. (15)  $\equiv f(\theta_1, \theta_2, \theta_3, L_3)$ , an equation for a branch of the singularity surface in actuated joint space of  $\theta_2, L_2$ , and  $L_3$  is obtained. Since  $2 \times 2 = 4$  overall solutions for  $\theta_1$  and  $\theta_3$  exist, a total of four branches are seen of the singularity surface in  $\theta_2$ - $L_2$ - $L_3$  actuated joint space. For the numerical example presented earlier in

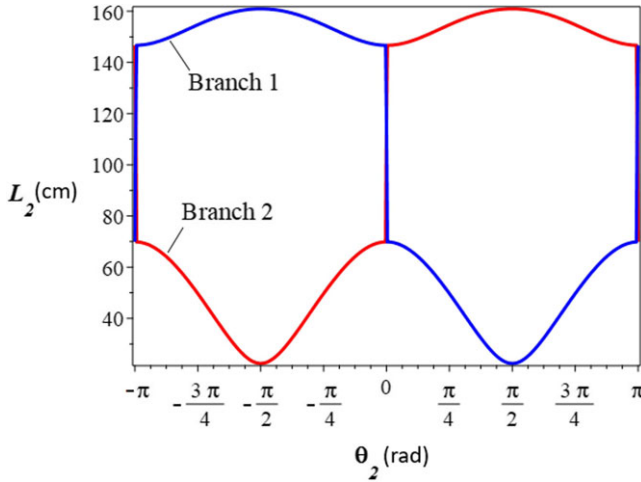


Figure 9. The two branches of the singularity curve in  $\theta_2$ - $L_2$  plane.

Section 5.2, the four branches of the singularity surface in  $\theta_2$ - $L_2$ - $L_3$  actuated joint space are depicted in Fig. 10.

Case 3:  $(j_{p64} j_{p55} - j_{p54} j_{p65}) = 0$

$$(j_{p64} j_{p55} - j_{p54} j_{p65}) = -\frac{3\sqrt{3}}{2}(h_1 - h_2)^2 L_4^2 \cos^2(\theta_5) \sin(\theta_4) = 0 \tag{82}$$

Clearly,  $h_1 = h_2$  gives a feasible design singularity. Additionally, the following singularities are also obtained:

- (1)  $L_4 = 0$
- (2)  $\theta_5 = (n + \frac{1}{2})\pi$  where  $n = 0, \pm 1, \pm 2, \dots$ , occurs when  $M_1H_1$  limb becomes parallel or antiparallel to the  $U_1$  axis
- (3)  $\theta_4 = n\pi$  where  $n = 0, \pm 1, \pm 2, \dots$ , occurs when  $M_1H_1$  limb comes in the plane of mid-platform M

Here, (b) yields the same singularity surface in  $L_4$ - $L_5$ - $L_6$  actuated joint space as shown in Fig. 12. From (c),  $|\cos(\theta_4)| = 1$ . So, using Eqs. (31) and (32):

$$s_5 = -\frac{f_2}{f_1} \tag{83}$$

$$c_5 = -\frac{g_2}{g_1 c_4} \tag{84}$$

$$\implies s_5^2 + c_5^2 = \left(\frac{f_2}{f_1}\right)^2 + \left(\frac{g_2}{g_1}\right)^2 = 1 \tag{85}$$

Thus, Eq. (85) gives the singularity surface in  $L_4$ - $L_5$ - $L_6$  actuated joint space. For the numerical example presented earlier in Section 5.2, the singularity surface is shown in Fig. 11.

Now, the “serial singularities” are analyzed occurring because the two platforms are serially connected by a serial kinematic chain. Consider the end-effector point to be at the centroid of platform H. The right-invariant angular velocity matrix  ${}^1\Omega_e$  is written as:

$${}^1\Omega_e = \dot{Q}(t) Q(t)^T \tag{86}$$

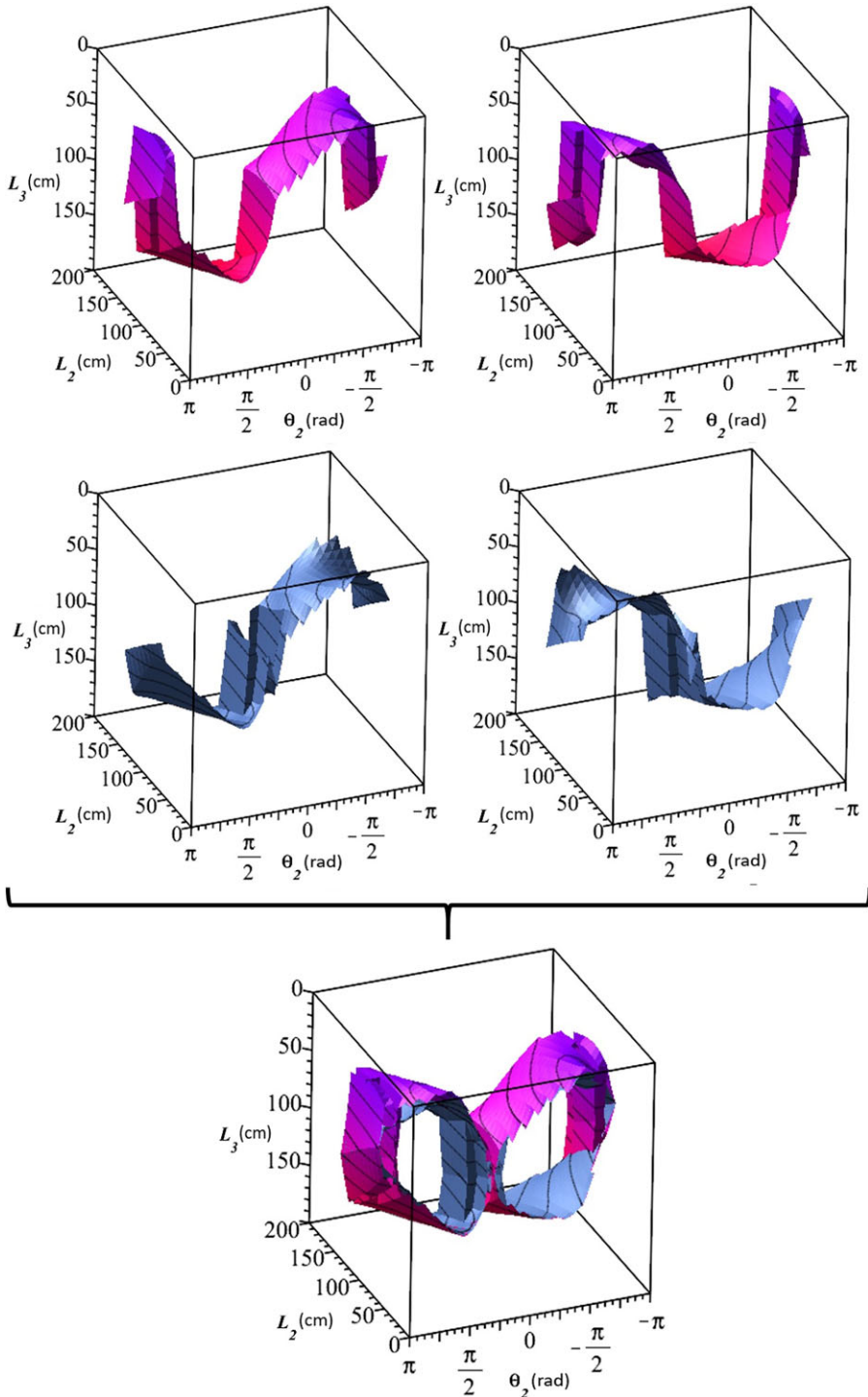


**Figure 10.** The four branches (left) and the overall singularity surface (right) in  $\theta_2$ - $L_2$ - $L_3$  actuated joint space.

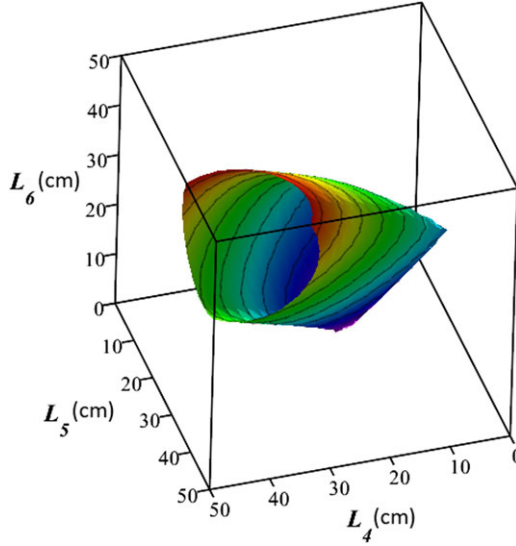


Figure 11. The singularity surface in  $L_4$ - $L_5$ - $L_6$  actuated joint space.

and extract from it the angular velocity vector of the end-effector  ${}^1\omega_e = [{}^1\Omega_{e_{3,2}}, {}^1\Omega_{e_{1,3}}, {}^1\Omega_{e_{2,1}}]^T$  since:

$${}^1\Omega_e = \begin{bmatrix} 0 & -{}^1\omega_{e_z} & {}^1\omega_{e_y} \\ {}^1\omega_{e_z} & 0 & -{}^1\omega_{e_x} \\ -{}^1\omega_{e_y} & {}^1\omega_{e_x} & 0 \end{bmatrix} \tag{87}$$

Now, the position vector of the end-effector is written as  ${}^8\mathbf{p}_e = [h_2, 0, 0, 1]^T$  and is transformed into base frame as  ${}^1\mathbf{p}_e = \mathbf{T} {}^8\mathbf{p}_e$ . Differentiating  ${}^1\mathbf{p}_e$  with respect to time, the velocity  ${}^1\mathbf{v}_e$  of end-effector  ${}^1\mathbf{p}_e$  is finally obtained as the first three entries (i.e., ignoring the fourth homogeneous coordinate) of  ${}^1\dot{\mathbf{p}}_e$ . Thus, now the twist  $\mathcal{S}_e$  of the platform H about the global coordinate system at the end-effector point can be found out by concatenating  ${}^1\omega_e$  and  ${}^1\mathbf{v}_e$ . Further simplification and rearranging gives the following equation:

$$\mathcal{S}_e = \mathbf{J}_s \dot{\mathbf{q}}(t) \tag{88}$$

where  $\mathbf{J}_s = \mathbf{J}_s(q(t))$  is another  $6 \times 6$  jacobian matrix with the following form (details in Section A.2):

$$\mathbf{J}_s = \begin{bmatrix} 0 & j_{s12} & j_{s13} & 0 & 0 & 0 \\ 0 & j_{s22} & j_{s23} & 0 & 0 & 0 \\ 1 & 0 & j_{s33} & 0 & 0 & 0 \\ j_{s41} & j_{s42} & j_{s43} & j_{s44} & j_{s45} & j_{s46} \\ j_{s51} & j_{s52} & j_{s53} & j_{s54} & j_{s55} & j_{s56} \\ 0 & j_{s62} & j_{s63} & j_{s64} & j_{s65} & j_{s66} \end{bmatrix} \tag{89}$$

Combining Eqs. (73) and (88), while assuming  $\mathbf{J}_p$  as nonsingular:

$$\mathcal{S}_e = \mathbf{J}_s \mathbf{J}_p^{-1} \mathbf{D} \dot{\Theta}(t) \tag{90}$$

Again, the matrix  $\mathbf{J}_s \mathbf{J}_p^{-1} \mathbf{D} \equiv \mathbf{J}_{eq}$  matrix definition given by Ghosal [35]. Thus, in accordance with the condition described in ref. [35], since  $\det(\mathbf{J}_{eq}) = 0$  if any one of  $\mathbf{J}_s$  or  $\mathbf{D}$  is singular,  $\det(\mathbf{J}_s) = 0$  and  $\det(\mathbf{D}) = 0$  give Type B (loss) singularity.

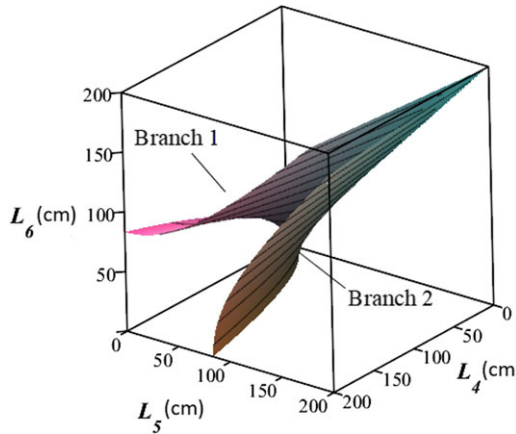


Figure 12. The two branches of the singularity surface in  $L_4$ - $L_5$ - $L_6$  actuated joint space.

6.2. Type B singularity: DOF-loss singularity

From  $\mathbf{D}$  matrix definition,  $\det(\mathbf{D}) = L_2 L_3 L_5 L_6 = 0$  gives the trivial conditions  $L_i = 0$  for  $i = 2, 3, 5, 6$  having obvious geometric interpretation (i.e., corresponding limb length becomes zero). Now, from Eq. (89), the determinant of  $\mathbf{J}_s$  matrix is

$$\det(\mathbf{J}_s) = ((j_{s44}j_{s55} - j_{s45}j_{s54})j_{s66} + (j_{s54}j_{s65} - j_{s55}j_{s64})j_{s46} + (j_{s45}j_{s64} - j_{s44}j_{s65})j_{s56}) \tag{91}$$

$$\cdot (j_{s12}j_{s23} - j_{s13}j_{s22}) \tag{92}$$

Substituting the expressions presented earlier for  $j_{s,xy}$  and further simplifying, the condition for singularity is written as:

$$\det(\mathbf{J}_s) = L_4^2 \sin(\theta_2) \cos(\theta_5) = 0 \tag{93}$$

Again,  $L_4 = 0$  is the trivial case. For the case  $\sin(\theta_2) = 0$ , the condition on  $\theta_2$  is

$$\theta_2 = n\pi \text{ where } n = 0, \pm 1, \pm 2, \dots \tag{94}$$

This has a straightforward geometric interpretation that whenever the  $R_2$  revolute joint (i.e.,  $\theta_2$ ) is actuated such that the axes of  $R_1$  and  $R_3$  (i.e.,  $Z_1$  and  $Z_3$ ) become parallel or antiparallel, this type of singularity occurs.

For the case  $\cos(\theta_5) = 0$ , the condition on  $\theta_5$  is

$$\theta_5 = \left(n + \frac{1}{2}\right)\pi \text{ where } n = 0, \pm 1, \pm 2, \dots \tag{95}$$

which implies that  $\sin(\theta_5) = \pm 1$ . Substituting in Eq. (31), two branches of the singularity surface in  $L_4$ - $L_5$ - $L_6$  actuated joint space are seen:

$$f_1 + f_2 = 0 \tag{96}$$

$$-f_1 + f_2 = 0 \tag{97}$$

since  $f_1$  and  $f_2$ , as defined in Eq. (33), are  $f(L_4, L_5, L_6)$ . For the numerical example presented earlier in Section 5.2, the two branches of the singularity surface are depicted in Fig. 12. Geometrically, this type of singularity is seen when  $M_1H_1$  limb becomes parallel or antiparallel to the  $U_{11}$  axis.

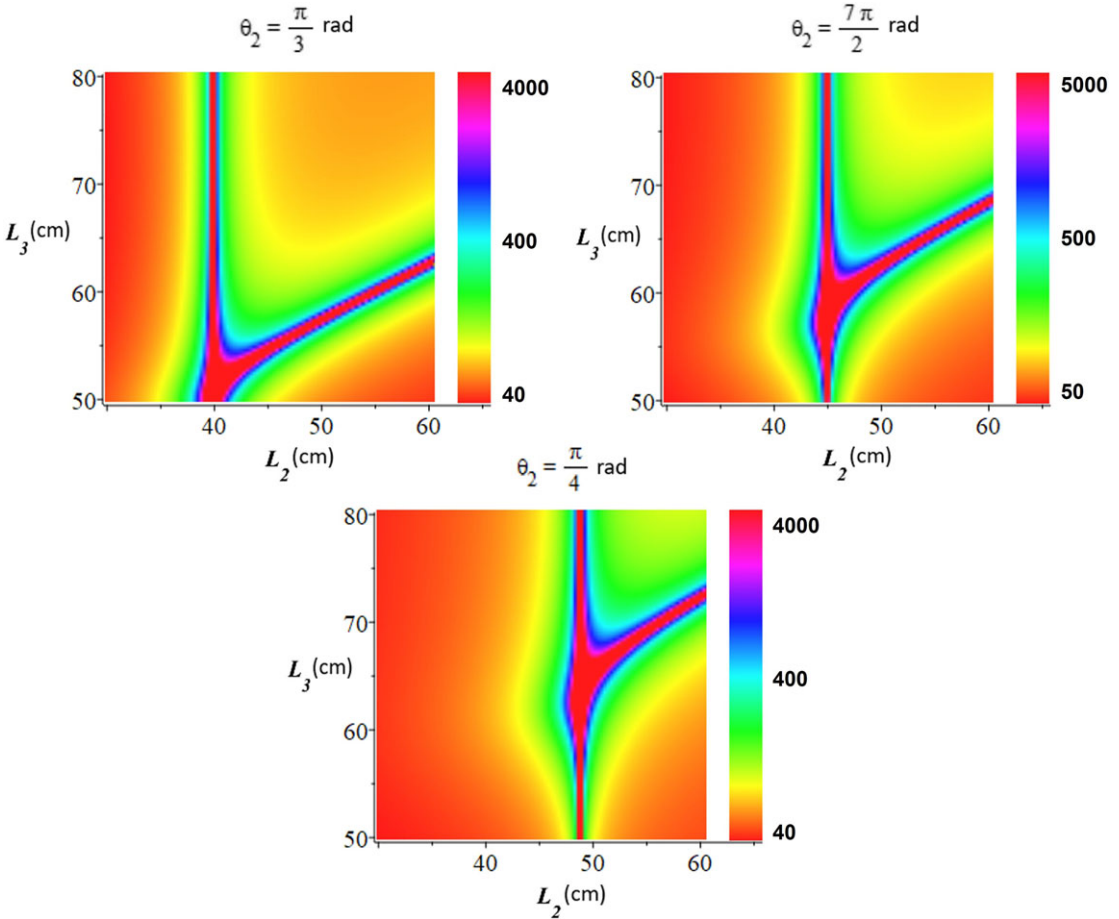


**Figure 13.** Manipulability index as a function of lower mechanism’s active joint variables for three different values of  $\theta_2$ .

**6.3. Type C singularity: special case**

As can be seen from Sections 6.1 and 6.2, singularities  $L_4 = 0$  and  $\theta_5 = \left(n + \frac{1}{2}\right) \pi$  satisfy the DOF-gain and DOF-loss conditions simultaneously. Hence, they are termed as the “special case” of singularities. This concludes the determination of the singularity conditions for the proposed hybrid manipulator.

**7. Kinematic manipulability and optimal design**

As seen in Section 6, the manipulator is in a singularity when the determinant of the Jacobian approaches zero. However, it is not desirable to even go close to being at a singularity when the manipulator is in motion. We use performance indicators such as dexterity and manipulability to quantify this “closeness” to a singularity. *Dexterity* (denoted as  $w_d$ ) is defined as the determinant of the manipulator Jacobian  $\mathbf{J}_{eq}$ , while *manipulability* (denoted as  $w_m$ ) is the square root of the determinant of the product of the manipulator Jacobian  $\mathbf{J}_{eq}$  by its transpose. However, since  $\mathbf{J}_{eq}$  is square, the dexterity and the manipulability are equal in magnitude:

$$w_m = |\det(\mathbf{J}_{eq})| \tag{98}$$



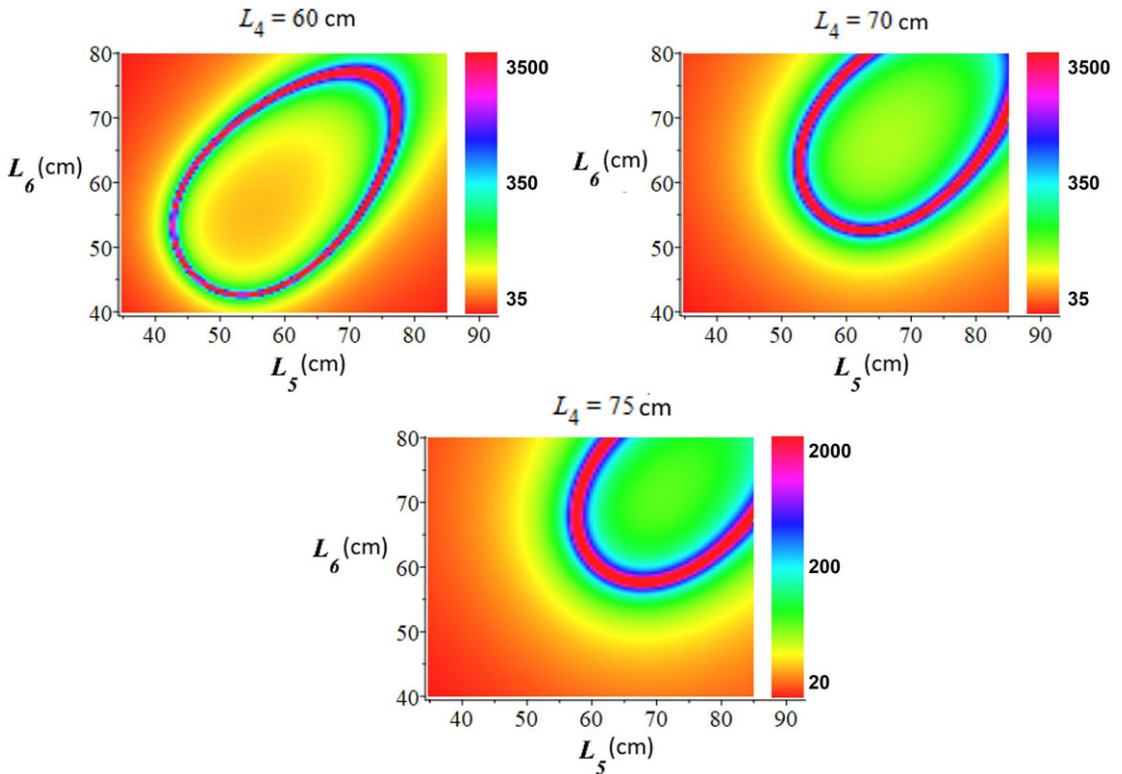


**Figure 14.** Manipulability index as a function of upper mechanism’s active joint variables for three different values of  $L_4$ .

The manipulability<sup>14</sup> index gets its importance from the fact that it represents the volume of the manipulability ellipsoid formed by the end-effector. A higher volume indicates it is more toward isotropy, while a vanishing volume signifies a singularity.

Consider the same design parameters and the active joint variables for the upper mechanism as in Section 5.2. The manipulability index as a function of the active joint variables of the lower mechanism for three different values of  $\theta_2$  has been plotted in Fig. 13.

Similarly, taking the same active joint variables for the lower mechanism as in Section 5.2, the manipulability index as a function of the active joint variables of the upper mechanism for three different values of  $L_4$  has been plotted in Fig. 14.

While a more rigorous optimization analysis could be done as in ref. [3] taking into account the workspace and condition number as well, we present, in this paper, a preliminary analysis to obtain an optimal design for the proposed hybrid manipulator considering just the kinematic manipulability as the determining factor. As can be seen from Figs. 13 and 14, for a given set of parameters, we have the manipulability varying in order of magnitude throughout the motion range. We define “optimal” design as the set of parameters with the highest minimum value of manipulability throughout the motion range, that is, which is farthest away from singularity for the entirety of its motion range. Therefore, we formulate the problem of optimal design as a bilevel nested continuous maximization–minimization problem:

$$\max_{L_1, b_2, b_{3x}, b_{3z}, h_1, h_2} \min_{L_2, L_3, L_4, L_5, L_6, \theta_2} w_m = \max_{\text{params}} \min_{\text{active}} w_m \tag{99}$$

<sup>14</sup>As reported here, it uses meters-seconds-radians in its units, specifically to maintain direct comparability with existing literature.

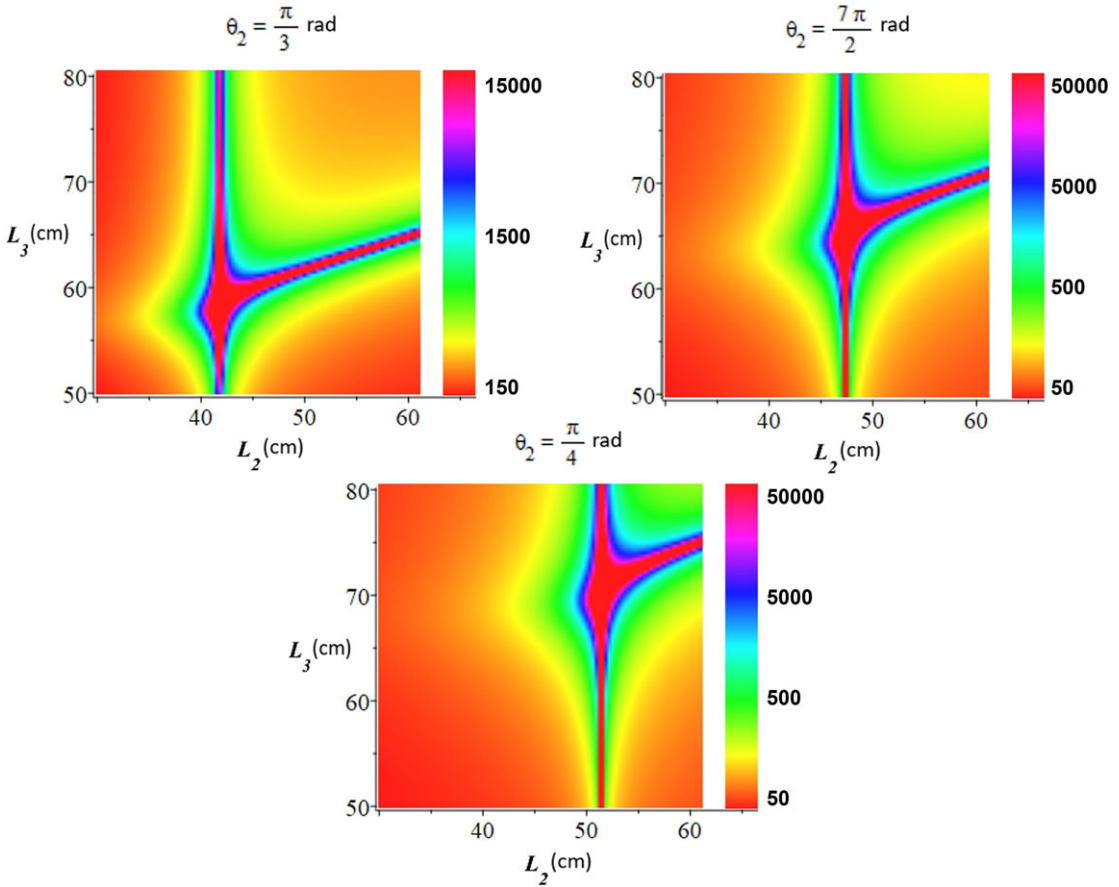


**Figure 15.** Manipulability index as a function of lower mechanism’s active joint variables for three different values of  $\theta_2$ , for optimal parameters.

This is clearly a high-dimensional complex problem. To make the analysis a bit simpler at the cost of losing full optimality, we split it into two lower-dimensional optimization problems as follows:

$$\max_{L_1, b_2, b_{3x}} \min_{L_2, L_3, \theta_2} w_m = \max_{\text{params}_1} \min_{\text{active}_{\text{lower}}} w_m \tag{100}$$

$$\max_{b_{3z}, h_1, h_2} \min_{L_4, L_5, L_6} w_m = \max_{\text{params}_2} \min_{\text{active}_{\text{upper}}} w_m \tag{101}$$

where  $\text{params} = \text{params}_1 \cup \text{params}_2$ ,  $\text{active} = \text{active}_{\text{lower}} \cup \text{active}_{\text{upper}}$ , wherein  $\text{params}_1 = \{L_1, b_2, b_{3x}\}$ ,  $\text{params}_2 = \{b_{3z}, h_1, h_2\}$ ,  $\text{active}_{\text{lower}} = \{L_2, L_3, \theta_2\}$ , and  $\text{active}_{\text{upper}} = \{L_4, L_5, L_6\}$ . Furthermore, we perform optimization using the MATLAB® Global Optimization Toolbox’s Genetic Algorithm solver. To further reduce computational complexity, we discretize the optimization with a small enough step size, and the parameters and the active variables are taken to be in a reasonably wide parameter range and motion range, respectively. For the optimization in Eq. (100), the parameters in  $\text{params}_2$  are assigned heuristically selected suitable values, and then for the optimization in Eq. (101),  $\text{params}_1$  are assigned their optimal values from Eq. (100). The optimization was carried out, resulting in the following solution:

$$\begin{aligned} L_1 &= 51.90 \text{ cm}; & b_2 &= 65.90 \text{ cm}; & b_{3x} &= 20.00 \text{ cm} \\ b_{3z} &= 62.70 \text{ cm}; & h_1 &= 42.40 \text{ cm}; & h_2 &= 34.80 \text{ cm} \end{aligned} \tag{102}$$

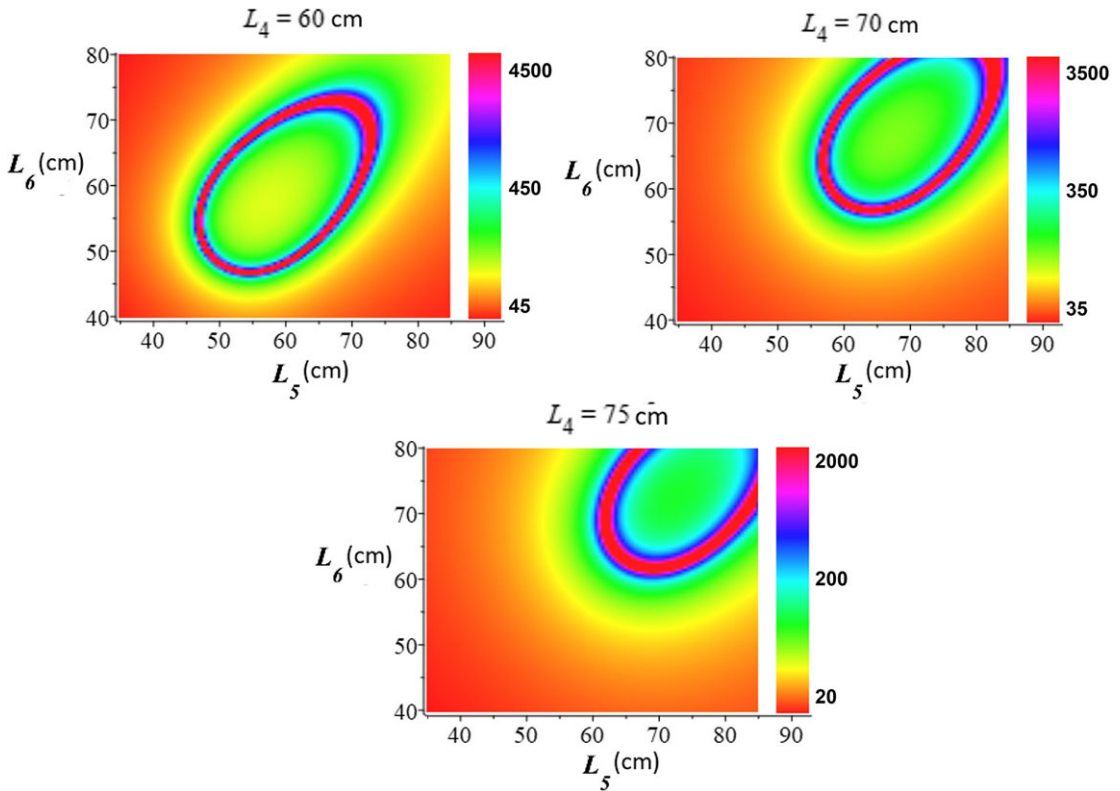


**Figure 16.** Manipulability index as a function of upper mechanism’s active joint variables for three different values of  $L_4$ , for optimal parameters.

Figures 15 and 16 show the manipulability index variation for the motion range for optimal parameters. It shows that the manipulability is pretty high in an appreciably large region of the motion range and how superior it is compared to Figs. 13 and 14 for the nonoptimal parameters.

### 8. Conclusion

This paper introduces a new 6-DOF hybrid manipulator, which uniquely combines a 1-RRR 2-SPS mechanism with a 3-UPU mechanism. This novel architecture holds promise for industrial settings that demand both translational motion and adjustable end-effector orientation. We have provided closed-form solutions for its forward and inverse kinematics, facilitating easier control and real-time applications. Performance and singularity analyses have also been conducted, leading us to a preliminary, near-optimal manipulator design.

Looking ahead, the manipulator’s potential can be further explored through real-time control algorithms and trajectory planning. A comprehensive workspace analysis could offer further insights into its practical applications. Lastly, a comparative study with other hybrid manipulators in the field would help benchmark its performance and identify improvement areas.

**Author contributions.** This paper presents the work of Sadanand Modak under the supervision of Dr. Rama Krishna K. This manuscript was prepared by Sadanand Modak and finalized (which includes a complete review and document organization) in collaboration with Dr. Rama Krishna K.

**Financial support.** This research received no specific grant from any funding agency, commercial, or not-for-profit sectors.

**Competing interests.** The author(s) declare none.

**Ethical approval.** Not applicable.

**Data availability statement.** Data sharing is not applicable to this article as no new data were created or analyzed in this study.

## References

- [1] R. Di Gregorio and V. Parenti-Castelli, "A Translational 3-DOF Parallel Manipulator," **In: *Advances in Robot Kinematics: Analysis and Control*** (J. Lenarčič and M. L. Husty, eds.) (Springer, Dordrecht, 1998) pp. 49–58.
- [2] L. W. Tsai, "Kinematics of a Three-DOF Platform with Three Extensible Limbs," **In: *Recent Advances in Robot Kinematics*** (J. Lenarčič and V. Parenti-Castelli, eds.) (Springer, Dordrecht, 1996) pp. 401–410.
- [3] L. W. Tsai and S. Joshi, "Kinematics and optimization of a spatial 3-UPU parallel manipulator," *J. Mech. Des. Trans. ASME* **122**(4), 439–446 (2000).
- [4] M. Karouia and J. Hervé, "A Three-DOF Tripod for Generating Spherical Rotation," **In: *Advances in Robot Kinematics*** (J. Lenarčič and M. M. Stanišić, eds.) (Springer, Dordrecht, 2000) pp. 395–402.
- [5] R. Di Gregorio, "Kinematics of the 3-UPU wrist," *Mech. Mach. Theory* **38**(3), 253–263 (2003).
- [6] C. M. Gosselin and J. Angeles, "Singularity analysis of closed-loop kinematic chains," *IEEE Trans. Robot. Autom.* **6**(3), 281–290 (1990).
- [7] R. Di Gregorio, "Kinematics analysis and singularities of novel decoupled parallel manipulators with simplified architecture," *Robotica* **35**(4), 961–979 (2017).
- [8] M. Russo and M. Ceccarelli, "A geometrical formulation for the workspace of parallel manipulators," *Robotica* **40**(8), 2581–2591 (2022).
- [9] S. Zarkandi, "Kinematic analysis and optimal design of a novel 3-PRR spherical parallel manipulator," *Proc. Inst. Mech. Eng. C J. Mech. Eng. Sci.* **235**(4), 693–712 (2021).
- [10] S. Zarkandi, "Kinematic analysis and workspace optimization of a novel 4RPSP +PS parallel manipulator," *Mech. Based Des. Struct. Mach.* **49**(1), 131–153 (2021).
- [11] Z. H. Li, Q. G. Lu, H. Z. Wang, Y. D. Huang, J. F. Liu, X. H. Zou and X. H. Zhan, "Design and analysis of a novel 3T1R four-degree-of-freedom parallel mechanism with infinite rotation capability," *Proc. Inst. Mech. Eng. C J. Mech. Eng. Sci.* **236**(14), 7771–7784 (2022).
- [12] R. Di Gregorio and V. Parenti-Castelli, "Mobility analysis of the 3-UPU parallel mechanism assembled for a pure translational motion," *J. Mech. Des. Trans. ASME* **124**(2), 259–264 (2002).
- [13] R. Di Gregorio, "Statics and singularity loci of the 3-UPU wrist," *IEEE Trans. Robot.* **20**(4), 630–635 (2004).
- [14] K. H. Hunt, "Structural kinematics of in-parallel-actuated robot-arms," *J. Mech. Transm. Autom. Des.* **105**(4), 705–712 (1983).
- [15] M. Shahinpoor, "Kinematics of a parallel-serial (Hybrid) manipulator," *J. Robot. Syst.* **9**(1), 17–36 (1992).
- [16] A. Singh, E. Singla, S. Soni and A. Singla, "Kinematic modeling of a 7-degree of freedom spatial hybrid manipulator for medical surgery," *Proc. Inst. Mech. Eng. H J. Eng. Med.* **232**(1), 12–23 (2018).
- [17] T. Maier and C. Woernle, "Inverse Kinematics for an Underconstrained Cable Suspension Manipulator," **In: *Advances in Robot Kinematics: Analysis and Control*** (J. Lenarčič and M. L. Husty, eds.) (Springer, Dordrecht, 1998) pp. 97–104.
- [18] P. Golla, S. Ramesh and S. Bandopadhyay, "Kinematics of the Hybrid 6-Axis (H6A) manipulator," *Robotica* **41**(8), 2251–2282 (2023).
- [19] L. Romdhane, "Design and analysis of a hybrid serial-parallel manipulator," *Mech. Mach. Theory* **34**(7), 1037–1055 (1999).
- [20] T. K. Tanev, "Kinematics of a hybrid (parallel–serial) robot manipulator," *Mech. Mach. Theory* **35**(9), 1183–1196 (2000).
- [21] X. Z. Zheng, H. Z. Bin and Y. G. Luo, "Kinematic analysis of a hybrid serial-parallel manipulator," *Int. J. Adv. Manuf. Technol.* **23**(11–12), 925–930 (2004).
- [22] J. Gallardo-Alvarado, "Kinematics of a hybrid manipulator by means of screw theory," *Multibody Syst. Dyn.* **14**(3), 345–366 (2005).
- [23] J. Gallardo-Alvarado, C. R. Aguilar-Nájera, L. Casique-Rosas, J. M. Rico-Martínez and M. N. Islam, "Kinematics and dynamics of 2 (3-RPS) manipulators by means of screw theory and the principle of virtual work," *Mech. Mach. Theory* **43**(10), 1281–1294 (2008).
- [24] B. Hu, "Formulation of unified jacobian for serial-parallel manipulators," *Robot. Comput. Integr. Manuf.* **30**(5), 460–467 (2014).
- [25] T. Huang, M. Li, X. M. Zhao, J. P. Mei, D. G. Chetwynd and S. J. Hu, "Conceptual design and dimensional synthesis for a 3-DOF module of the TriVariant-a novel 5-DOF reconfigurable hybrid robot," *IEEE Trans. Robot.* **21**(3), 449–456 (2005).
- [26] Y. Lu, C. Zhang, C. Cao, Y. Dong and Y. Liu, "Kinematics and dynamics of a novel hybrid manipulator," *Proc. Inst. Mech. Eng. C J. Mech. Eng. Sci.* **230**(10), 1644–1657 (2016).
- [27] V. Sangveraphunsiri and K. Chooprasird, "Dynamics and control of a 5-DOF manipulator based on an H-4 parallel mechanism," *Int. J. Adv. Manuf. Technol.* **52**(1–4), 343–364 (2011).
- [28] L. Xu, Q. Chen, L. He and Q. Li, "Kinematic analysis and design of a novel 3T1R 2-(PRR) 2RH hybrid manipulator," *Mech. Mach. Theory* **112**(1), 105–122 (2017).

[29] P. Xu, C. F. Cheung, B. Li, L. T. Ho and J. F. Zhang, “Kinematics analysis of a hybrid manipulator for computer controlled ultra-precision freeform polishing,” *Robot. Comput. Integr. Manuf.* **44**(1), 44–56 (2017).  
 [30] W. Guo, R. Li, C. Cao and Y. Gao, “Kinematics analysis of a novel 5-DOF hybrid manipulator,” *Int. J. Automat. Technol.* **9**(6), 765–774 (2015).  
 [31] J. He, H. Zheng, F. Gao and H. Zhang, “Dynamics and control of a 7-DOF hybrid manipulator for capturing a non-cooperative target in space,” *Mech. Mach. Theory* **140**(1), 83–103 (2019).  
 [32] G. Carbone and M. Ceccarelli, “A stiffness analysis for a hybrid parallel-serial manipulator,” *Robotica* **22**(5), 567–576 (2004).  
 [33] T. Yoshikawa, *Foundations of Robotics: Analysis and Control* (MIT Press, Cambridge, MA, 1990).  
 [34] S. K. Saha, *Introduction to Robotics* (Tata McGraw-Hill Education, New Delhi, 2014).  
 [35] A. Ghosal, *Robotics: Fundamental Concepts and Analysis* (Oxford University Press, Oxford, 2006).

## A. Appendix

### A.1. Calculating overall transformation matrix

The overall transformation matrix is written using the D-H Tables I and II as:<sup>15</sup>

$$\mathbf{T}_1 \equiv {}^1_4[\mathbf{T}] = {}^1_2[\mathbf{T}]_3^2[\mathbf{T}]_4^3[\mathbf{T}] \tag{A1}$$

$$\mathbf{T}_2 \equiv {}^4_8[\mathbf{T}] = {}^4_5[\mathbf{T}]_6^5[\mathbf{T}]_7^6[\mathbf{T}]_8^7[\mathbf{T}] \tag{A2}$$

$$\therefore \mathbf{T} = \mathbf{T}_1 \mathbf{C}_u^l \mathbf{T}_2 = \begin{bmatrix} t_{11} & t_{12} & t_{13} & t_{14} \\ t_{21} & t_{22} & t_{23} & t_{24} \\ t_{31} & t_{32} & t_{33} & t_{34} \\ 0 & 0 & 0 & 1 \end{bmatrix} \tag{A3}$$

where,

$$t_{11} = \frac{1}{2}(c_1c_2c_3 + s_1s_3 - \sqrt{3}c_1s_2);$$

$$t_{12} = s_1c_3 - c_1c_2s_3;$$

$$t_{13} = -\frac{1}{2}(c_1s_2 + \sqrt{3}(c_1c_2c_3 + s_1s_3));$$

$$t_{21} = \frac{1}{2}(s_1c_2c_3 - c_1s_3 - \sqrt{3}s_1s_2);$$

$$t_{22} = -c_1c_3 - s_1c_2s_3;$$

$$t_{23} = -\frac{1}{2}(s_1s_2 - \sqrt{3}(c_1s_3 - s_1c_2c_3));$$

$$t_{31} = -\frac{1}{2}(\sqrt{3}c_2 + s_2c_3);$$

$$t_{32} = s_2s_3;$$

$$t_{33} = \frac{1}{2}(\sqrt{3}s_2c_3 - c_2);$$

<sup>15</sup>In this paper, the shorthand notation  $c_k = \cos \theta_k$  and  $s_k = \sin \theta_k$  is adopted. All the symbolic and numerical computations presented have been performed using Maple™.

$$\begin{aligned}
 t_{14} &= ((c_3c_4 - 2s_3s_4)c_2c_5 - s_2s_5) c_1 + (2c_3s_4 + s_3c_4)s_1c_5 \frac{L_4}{2} - L_1s_1 \\
 &\quad - \frac{\sqrt{3}}{2} ((c_2c_3s_5 + s_2c_4c_5)c_1 + s_1s_3s_5) L_4; \\
 t_{24} &= ((c_3c_4 - 2s_3s_4)s_1c_2 - (2c_3s_4 + s_3c_4)c_1) c_5 - s_1s_2s_5 \frac{L_4}{2} + L_1c_1 \\
 &\quad + \frac{\sqrt{3}}{2} ((c_1s_3 - s_1c_2c_3)s_5 - s_1s_2c_4c_5) L_4; \\
 t_{34} &= - \left( \sqrt{3}(c_2c_4c_5 - s_2c_3s_5) + (c_3c_4 - 2s_3s_4)s_2c_5 + c_2s_5 \right) \frac{L_4}{2};
 \end{aligned} \tag{A4}$$

**A.2. Singularity matrices**

The  $\mathbf{J}_p = \mathbf{J}_p(q(t))$  is a  $6 \times 6$  jacobian matrix having the following form:

$$\mathbf{J}_p = \begin{bmatrix} 0 & 1 & 0 & 0 & 0 & 0 \\ j_{p21} & j_{p22} & 0 & 0 & 0 & 0 \\ j_{p31} & j_{p32} & j_{p33} & 0 & 0 & 0 \\ 0 & 0 & 0 & 0 & 0 & 1 \\ 0 & 0 & 0 & j_{p54} & j_{p55} & j_{p56} \\ 0 & 0 & 0 & j_{p64} & j_{p65} & j_{p66} \end{bmatrix} \tag{A5}$$

wherein,

$$\begin{aligned}
 j_{p21} &= b_2(L_1c_1 - \sqrt{3}h_1s_1s_2); \\
 j_{p31} &= \frac{b_{3x}}{2} \left( -\sqrt{3}h_1s_1s_2 + 3h_1s_1c_2c_3 - 3h_1c_1s_3 + 2L_1c_1 \right); \\
 j_{p22} &= \sqrt{3}h_1b_2c_1c_2; \\
 j_{p32} &= \frac{h_1}{2} \left( \sqrt{3}b_{3x}c_1c_2 + 3b_{3x}c_1s_2c_3 - \sqrt{3}b_{3z}s_2 + 3b_{3z}c_2c_3 \right); \\
 j_{p33} &= -\frac{3h_1}{2} \left( (b_{3x}s_1 + L_1)c_3 + (-b_{3x}c_1c_2 + b_{3z}s_2)s_3 \right); \\
 j_{p54} &= \frac{3}{2}(h_1 - h_2)L_4s_4c_5; \\
 j_{p55} &= \frac{L_4}{2}(h_1 - h_2) \left( 3c_4s_5 - \sqrt{3}c_5 \right); \\
 j_{p56} &= \frac{1}{2} \left( 2L_4 - \sqrt{3}(h_1 - h_2)s_5 - 3(h_1 - h_2)c_4c_5 \right); \\
 j_{p64} &= \frac{3}{2}(h_1 - h_2)L_4s_4c_5; \\
 j_{p65} &= \frac{L_4}{2}(h_1 - h_2) \left( 3c_4s_5 + \sqrt{3}c_5 \right); \\
 j_{p66} &= \frac{1}{2} \left( 2L_4 + \sqrt{3}(h_1 - h_2)s_5 - 3(h_1 - h_2)c_4c_5 \right);
 \end{aligned} \tag{A6}$$

The  $\mathbf{J}_s = \mathbf{J}_s(q(t))$  is another  $6 \times 6$  jacobian matrix with the following form:

$$\mathbf{J}_s = \begin{bmatrix} 0 & j_{s12} & j_{s13} & 0 & 0 & 0 \\ 0 & j_{s22} & j_{s23} & 0 & 0 & 0 \\ 1 & 0 & j_{s33} & 0 & 0 & 0 \\ j_{s41} & j_{s42} & j_{s43} & j_{s44} & j_{s45} & j_{s46} \\ j_{s51} & j_{s52} & j_{s53} & j_{s54} & j_{s55} & j_{s56} \\ 0 & j_{s62} & j_{s63} & j_{s64} & j_{s65} & j_{s66} \end{bmatrix} \tag{A7}$$

wherein,

$$\begin{aligned} j_{s12} &= -s_1; \\ j_{s13} &= -c_1s_2; \\ j_{s22} &= c_1; \\ j_{s23} &= -s_1s_2; \\ j_{s33} &= -c_2; \\ j_{s41} &= \frac{1}{2} \left( \sqrt{3} \left( (c_2c_3s_5 + s_2c_4c_5)s_1 - c_1s_3s_5 \right) L_4 + h_2s_1s_2 \right) - h_2s_1c_2c_3 + (h_2s_3 - 2L_1)c_1 \\ &\quad + \frac{L_4}{2} \left( (2s_3s_4 - c_3c_4)c_2c_5 + s_2s_5 \right) s_1 + (2c_3s_4 + s_3c_4)c_1c_5; \\ j_{s42} &= -\frac{c_1}{2} \left( \sqrt{3}L_4(c_2c_4c_5 - s_2c_3s_5) + L_4(s_2c_3c_4c_5 + c_2s_5 - 2s_2s_3s_4c_5) + h_2(\sqrt{3}c_2 + s_2c_3) \right); \\ j_{s43} &= \frac{1}{2} \left( \left( \sqrt{3}L_4s_5 - h_2 \right) (c_1c_2s_3 - s_1c_3) - L_4c_5 (c_1c_2(2c_3s_4 + s_3c_4) - s_1(c_3c_4 - 2s_3s_4)) \right); \\ j_{s44} &= \frac{1}{2}L_4c_5 \left( \sqrt{3}c_1s_2s_4 - (c_3s_4 + 2s_3c_4)c_1c_2 - (s_3s_4 - 2c_3c_4)s_1 \right); \\ j_{s45} &= -\frac{L_4}{2} \left( \sqrt{3} \left( (c_2c_3c_5 - s_2c_4s_5)c_1 + s_1s_3c_5 \right) + ((c_3c_4 - 2s_3s_4)c_2s_5 + s_2c_5) c_1 \right) \\ &\quad - \frac{L_4}{2} \left( (2c_3s_4 + s_3c_4)s_1s_5 \right); \\ j_{s46} &= \frac{1}{2} \left( (2c_3s_4 + s_3c_4)s_1c_5 - \sqrt{3} \left( (c_2c_3s_5 + s_2c_4c_5)c_1 + s_1s_3s_5 \right) \right) \\ &\quad + \frac{1}{2} \left( ((c_3c_4 - 2s_3s_4)c_2c_5 - s_2s_5) c_1 \right); \\ j_{s51} &= \frac{1}{2} \left( (c_1c_2c_3 + s_1s_3)h_2 - \sqrt{3} \left( (c_2c_3s_5 + s_2c_4c_5)c_1 + s_1s_3s_5 \right) L_4 + h_2c_1s_2 \right) \\ &\quad + \frac{1}{2} \left( ((c_3c_4 - 2s_3s_4)c_2c_5 - s_2s_5) c_1 + (2c_3s_4 + s_3c_4)s_1c_5 \right) L_4 - 2L_1s_1; \\ j_{s52} &= -\frac{s_1}{2} \left( \sqrt{3}L_4(c_2c_4c_5 - s_2c_3s_5) + L_4(s_2c_3c_4c_5 + c_2s_5 - 2s_2s_3s_4c_5) + h_2(\sqrt{3}c_2 + s_2c_3) \right); \end{aligned} \tag{A8}$$

$$\begin{aligned}
j_{s53} &= \frac{1}{2} \left( (\sqrt{3}L_4s_5 - h_2) (s_1c_2s_3 + c_1c_3) - L_4c_5 (2s_4(s_1c_2c_3 - c_1s_3) + c_4(s_1c_2s_3 + c_1c_3)) \right); \\
j_{s54} &= \frac{1}{2}L_4c_5 \left( \sqrt{3}s_1s_2s_4 - (c_3s_4 + 2s_3c_4)s_1c_2 + (s_3s_4 - 2c_3c_4)c_1 \right); \\
j_{s55} &= -\frac{L_4}{2} \left( \sqrt{3} ((c_2c_3c_5 - s_2c_4s_5)s_1 - c_1s_3c_5) + ((c_3c_4 - 2s_3s_4)c_2s_5 + s_2c_5) s_1 \right) \\
&\quad + \frac{L_4}{2} ((2c_3s_4 + s_3c_4)c_1s_5); \\
j_{s56} &= \frac{1}{2} \left( \sqrt{3} ((c_1s_3 - s_1c_2c_3)s_5 - s_1s_2c_4c_5) + ((c_3c_4 - 2s_3s_4)s_1c_2 - (2c_3s_4 + s_3c_4)c_1) c_5 \right) \\
&\quad - \frac{1}{2} (s_1s_2s_5); \\
j_{s62} &= \frac{1}{2} \left( \sqrt{3} ((c_2c_3s_5 + s_2c_4c_5)L_4 + h_2s_2) + (s_2s_5 - (c_3c_4 - 2s_3s_4)c_2c_5) L_4 - h_2c_2c_3 \right); \\
j_{s63} &= \frac{s_2}{2} \left( (c_4c_5 - \sqrt{3}s_5)L_4s_3 + 2L_4c_3s_4c_5 + h_2s_3 \right); \\
j_{s64} &= \frac{1}{2}L_4c_5 \left( \sqrt{3}c_2s_4 + s_2c_3s_4 + 2s_2s_3c_4 \right); \\
j_{s65} &= \frac{L_4}{2} \left( \sqrt{3}(c_2c_4s_5 + s_2c_3c_5) + (c_3c_4 - 2s_3s_4)s_2s_5 - c_2c_5 \right); \\
j_{s66} &= \frac{1}{2} \left( \sqrt{3}(s_2c_3s_5 - c_2c_4c_5) - (c_3c_4 - 2s_3s_4)s_2c_5 - c_2s_5 \right) \tag{A9}
\end{aligned}$$